nature structural & molecular biology

Article

https://doi.org/10.1038/s41594-024-01450-z

Ribosomal A-site interactions with near-cognate tRNAs drive stop codon readthrough

Received: 28 May 2023

Accepted: 12 November 2024

Published online: 13 January 2025

Check for updates

Zuzana Čapková Pavlíková[1,2,9], Petra Miletínová[1,9], Adriana Roithová[1], Klára Pospíšilová[1], Kristína Záhonová[3,4,5,6], Ambar Kachale[3,7], Thomas Becker[8], Ignacio M. Durante[3,7], Julius Lukeš[3,7], Zdeněk Paris[3,7], Petra Beznosková[1] & Leoš Shivaya Valášek[1]

Transfer RNAs (tRNAs) serve as a dictionary for the ribosome translating the genetic message from mRNA into a polypeptide chain. In addition to this canonical role, tRNAs are involved in other processes such as programmed stop codon readthrough (SC-RT). There, tRNAs with near-cognate anticodons to stop codons must outcompete release factors and incorporate into the ribosomal decoding center to prevent termination and allow translation to continue. However, not all near-cognate tRNAs promote efficient SC-RT. Here, with the help of *Saccharomyces cerevisiae* and *Trypanosoma brucei*, we demonstrate that those tRNAs that promote efficient SC-RT establish critical contacts between their anticodon stem (AS) and ribosomal proteins Rps30/eS30 and Rps25/eS25 forming the decoding site. Unexpectedly, the length and well-defined nature of the AS determine the strength of these contacts, which is reflected in organisms with reassigned stop codons. These findings open an unexplored direction in tRNA biology that should facilitate the design of artificial tRNAs with specifically altered decoding abilities.

Occurrence of a stop codon in the decoding site (A-site) of the elongating ribosome triggers uneven competition between the termination ternary complex, composed of eukaryotic release factors eRF1 and eRF3 and guanosine triphosphate (GTP), and near-cognate tRNAs recognizing two of the three bases of any of the three stop codons, as previously reviewed[1]. Higher energetic stability of the interaction between the UAG, UAA or UGA stop codon and the eRF1–eRF3–GTP complex in comparison to a corresponding near-cognate tRNA favors the former competitor in 99.9% of cases[2]. Stop codon recognition by eRF1 then stimulates GTP hydrolysis on eRF3, upon which eRF1 with the assistance of the ATPase ABCE1 (adenosine triphosphate-binding cassette subfamily E member 1) mediates the release of the nascent peptide[3–5]. The post-termination complex is then disassembled, enabling its constituents to participate in further rounds of translation.

In the remaining 0.1% of cases, near-cognate tRNAs usurp the stop codon to avoid termination and instead allow so-called stop codon

[1]Laboratory of Regulation of Gene Expression, Institute of Microbiology, Czech Academy of Sciences, Prague, Czech Republic. [2]Faculty of Science, Charles University, Prague, Czech Republic. [3]Institute of Parasitology, Biology Centre, Czech Academy of Sciences, České Budějovice (Budweis), Czech Republic. [4]Department of Parasitology, Faculty of Science, Charles University, BIOCEV, Vestec, Czech Republic. [5]Life Science Research Centre, Faculty of Science, University of Ostrava, Ostrava, Czech Republic. [6]Division of Infectious Diseases, Department of Medicine, Faculty of Medicine and Dentistry, University of Alberta, Edmonton, Alberta, Canada. [7]Faculty of Sciences, University of South Bohemia, České Budějovice (Budweis), Czech Republic. [8]Department of Biochemistry, Gene Center, University of Munich, Munich, Germany. [9]These authors contributed equally: Zuzana Čapková Pavlíková, Petra Miletínová. e-mail: valasekl@biomed.cas.cz

readthrough (SC-RT), as previously reviewed[6,7]. As a result, C-terminally extended proteins are produced either as an infrequent failure of the system or, if programmed by various features acting in *trans* and/or in *cis*, as a desirable variant of a given protein with newly acquired functional qualities and/or cellular localization. Among the latter features belong the identity of the stop codon and surrounding sequence contexts[2,8–11], proximal RNA structures[12], RNA modifications[13,14], presence of RNA-binding proteins[15] and eukaryotic initiation factor eIF3 (refs. 16,17) and the availability and quality of aminoacylated (aa) near-cognate tRNAs[18–21].

Interestingly, not all near-cognate tRNAs are capable of promoting efficient SC-RT[18,21]. Those that can are called readthrough inducing (rti)-tRNAs and, at least in *Saccharomyces cerevisiae*, include $tRNA^{Trp}_{CCA}$ and $tRNA^{Cys}_{GCA}$ for UGA with the third-base wobble, the M isoacceptor of $tRNA^{Gln}$ for UAG ($tRNA^{Gln}_{CUG}$[M]) with the first-base wobble and $tRNA^{Tyr}_{GUA}$ for UAR (UAA and UAG collectively) stop codons with the third-base wobble[19,20]. Virtually nothing is known about the qualities that notably increase the odds of rti-tRNAs competing with eRF1 for the stop codon or about the underlying molecular mechanism of their preferred selection by the decoding center.

One hypothesis to understand how the rti-tRNAs get accepted by the ribosome that is poised to terminate can be found in analogy with the third-base wobbling during elongation. Cognate codon–anticodon recognition in the decoding center of the ribosome is read out by the two conserved decoding bases (A1492 and A1493 in bacteria), which are flipped out of helix 44 (h44) of 18S rRNA to check a proper A-helix minor grove geometry of the mRNA:tRNA decoding complex. A cognate complex then induces a conformational change in the ribosomal small subunit, referred to as domain closure[22,23]. This movement was proposed to induce a tighter fit around the codon–anticodon minihelix and to help activate GTP hydrolysis on eukaryotic elongation factor 1A (eEF1A). Domain closure appears to be a specific response to aa-tRNA selection and does not occur in the presence of eRF1 (ref. 24). Because the h44 decoding bases sense indirectly only the first two codon pairs, enabling the +3 position to participate in the wobble interactions[25], the same architecture is believed to be induced with near-cognate tRNAs[26]. In other words, to be selected, near-cognate tRNAs have to go through the same activated state as fully cognate tRNAs. However, in physiological conditions, the probability of reaching the activated state is much more favored for the cognate interactions than for the near-cognate ones[24], which is reflected in increased ribosome occupancy at the wobble codons[27,28]. The same is most likely true for tRNAs near-cognate to the stop codons with the third-base wobble regardless of their ability to boost SC-RT.

The situation might be even more complicated with near-cognate tRNAs with the first-base wobble, of which $tRNA^{Gln}_{CUG}$[M] is a very potent inducer of SC-RT compared to others from the same family, such as $tRNA^{Arg}$, $tRNA^{Glu}$, $tRNA^{Gly}$ and $tRNA^{Lys}$ (refs. 18,19,21). Given these differences, it is clear that, in addition to the minor groove geometry check carried out by specific 18S rRNA bases, other factors influence the tRNA selection process, providing rti-tRNAs with the advantage of being selected at a much higher frequency than other near-cognate tRNAs. For example, in addition to 18S rRNA, four small ribosomal proteins, namely Rps23/uS12, Rps15/uS19, Rps25/eS25 and Rps30/eS30, are part of the decoding site, with all of them having profound roles during codon sampling[24,29–31]. To name a few, it was proposed that the contacts with the codon–anticodon minihelix made by Rps15/uS19 and especially by Rps30/eS30 could increase the stability of aa-tRNAs during initial selection and accommodation[24,29]. Therefore, the question arises whether ribosomal proteins could have a discriminatory role.

Another factor that may influence SC-RT could lie directly in the nature of the tRNA backbone. Indeed, we recently showed that $tRNA^{Trp}_{CCA}$ with a short anticodon stem (AS; 4 bp instead of the canonical 5 bp), which occurs naturally in several protists with all three stop codons reassigned to sense codons, markedly boosts SC-RT on UGA[32]. Curiously, this special quality of the 4-bp $tRNA^{Trp}_{CCA}$ originating outside of the anticodon loop represents one of the critical life-sustaining measures in these organisms with an altered genetic code.

Here, with help of the $tRNA^{Gln}_{CUG}$[M], $tRNA^{Trp}_{CCA}$ and $tRNA^{Cys}_{GCA}$, we show that both the length and the nature of the AS (in particular, the base composition of its fourth 28:42 bp) critically contribute to the increased propensity of rti-tRNAs to SC-RT on UAR and UGA, respectively, at least in *S. cerevisiae* and *Trypanosoma brucei*. Bioinformatics analyses revealed that ciliates with UAR-to-glutamine reassignment have genomic bias toward this particular base-pair composition with pyrimidine 28 and purine 42 of their $tRNA^{Gln}_{UUG}$. Yeast genetics identified contacts that ASs of these rti-tRNAs and of rti-$tRNA^{Tyr}_{GUA}$ establish with specific amino acid residues of Rps30/eS30 and Rps25/eS25, respectively. Disruption of these contacts greatly affects SC-RT-promoting potential that these rti-tRNAs normally allow. Therefore, we propose that, in addition to the degree of complementarity of the codon–anticodon minihelix and its interactions with the specific 18S rRNA decoding bases, tRNAs establish additional contacts with the decoding center components through their backbone, particularly through their AS. These so-far-unrecognized interactions could further propagate a tighter fit around the codon–anticodon minihelix, thereby increasing the likelihood that both cognate and specific near-cognate aa-tRNAs reach an activated state to be selected.

Results

Primary sequence of $tRNA^{Gln}$ determines the SC-RT efficiency

We previously observed that, whereas $tRNA^{Gln}_{CUG}$[M] isoacceptor dramatically induced SC-RT at all four UAG-N tetranucleotides, the other $tRNA^{Gln}_{UUG}$ isoacceptors, such as $tRNA^{Gln}_{UUG}$[B] and $tRNA^{Gln}_{UUG}$[L], promoted SC-RT at their corresponding near-cognate UAA-N tetranucleotides only marginally[19]. Remarkably, the nuclear genome of the budding yeast *S. cerevisiae* contains altogether ten genes encoding $tRNA^{Gln}$. Whereas nine of them encode different isodecoders of the UUG anticodon isoacceptor, there is only a single gene encoding the CUG anticodon $tRNA^{Gln}_{CUG}$[M] isoacceptor. Apart from the distinct anticodons of $tRNA^{Gln}_{CUG}$[M] versus the remaining nine UUG isodecoders, there are only minor variations in their backbone sequence embodied by three specific bases. These are A versus G at position 42 of the AS of the M isoacceptor (also present in the $tRNA^{Gln}_{UUG}$[E2] isodecoder), A versus G at position 51 in the pseudouridine (T) loop and G versus A at position 66 in the acceptor stem (Fig. 1a and Extended Data Fig. 1). Notably, none of these bases is subject to otherwise widespread tRNA modifications (https://www.tmodbase.com)[33,34]. These differences prompted us to investigate the mechanistic basis for the elevated SC-RT-inducing potential of the $tRNA^{Gln}_{CUG}$[M] isoacceptor. We wondered whether this is because of the differing anticodon and its modified nucleotide(s) or because of nucleotide variations in the primary sequence of the $tRNA^{Gln}$ backbone.

To test the impact of each anticodon, we took the M and L isoacceptors (identical in the backbone sequence with the exception of the aforementioned bases) and simply swapped their anticodons, creating the mutant $tRNA^{Gln}_{U^*UG}[M]^{A42;A51;G66}$ and $tRNA^{Gln}_{C^*UG}[L]^{G42;G51;A66}$ forms. Next, we expressed them individually (along with the wild-type (wt) $tRNA^{Gln}_{UUG}$[B] and $tRNA^{Gln}_{UUG}$[E2] isodecoders) in yeast cells and measured the SC-RT efficiency using our well-established dual-luciferase system[19], featuring *Renilla* and firefly luciferases set in the same frame but separated by either the UAG or UAA stop codons. We confirmed markedly induced SC-RT of $tRNA^{Gln}_{CUG}$[M] at UAG-C (Fig. 1b). In addition, we observed that substituting its anticodon from CUG to UUG ($tRNA^{Gln}_{U^*UG}[M]^{A42;A51;G66}$) did not impair the ability of this anticodon-swapped mutant $tRNA^{Gln}$ to promote efficient SC-RT also on UAA (Fig. 1c). Please note that absolute values are not comparable between experiments shown in Fig. 1b,c because the intrinsic ability of stop codons to allow natural readthrough differs among them, with UGA being the most readthrough-permissive stop codon and UAA being the

https://doi.org/10.1038/s41594-024-01450-z

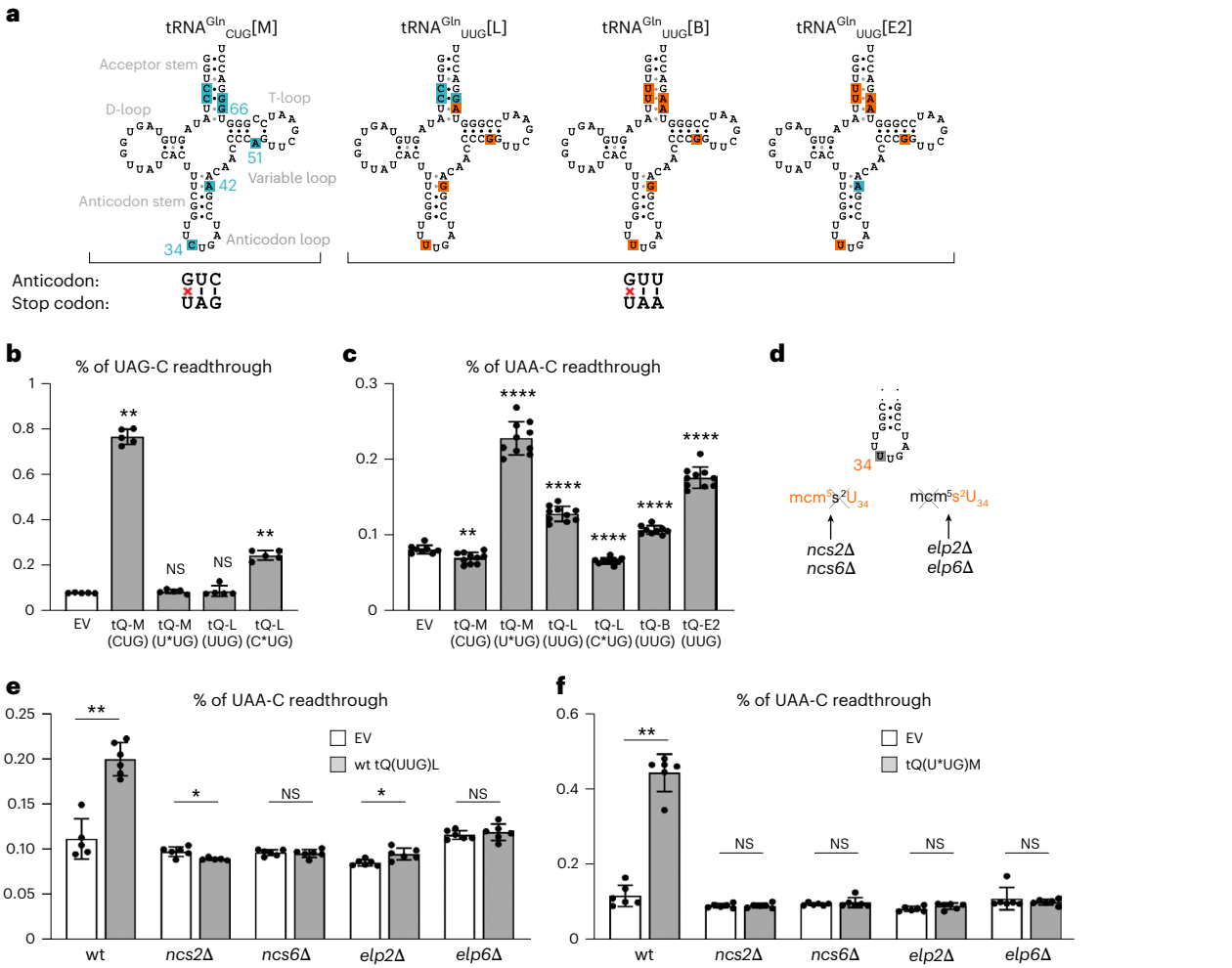

Fig. 1 | Neither anticodons nor modifications determine the SC-RT efficiency of tRNA^{Gln}. a, Predicted secondary structures of all tRNA^{Gln} studied herein (GtRNAdb[60]). The bases differing between the CUG and UUG isoacceptors are shown in blue and orange, respectively. **b**,**c**, The anticodon of tRNA^{Gln} does not impact the SC-RT efficiency. The wt and indicated (*) mutant CUG or UUG tRNA^{Gln} isoacceptors with swapped anticodons were expressed individually (along with an EV) in wt yeast cells and SC-RT efficiency on UAG-C (**b**) or UAA-C (**c**) was measured using the dual-luciferase system (Methods). Readthrough values were normalized to the control CAA cells and plotted as a percentage of readthrough. Each bar is represented by $n = 5$ (**b**) or $n \geq 9$ (**c**) readthrough values (individual biological replicates shown as dots) and illustrates the mean value ± s.d. Statistical significance was determined using the nonparametric Mann–Whitney test. $^{****}P < 0.0001$, $^{***}P < 0.001$, $^{**}P < 0.01$ and $^{*}P < 0.05$; NS, nonsignificant. For source data of Firefly and Renilla measurements, additional measurements and statistical calculations, see Source Data Fig. 1. **d**, Scheme indicating the nature of the tRNA$^{Gln}_{UUG}$ anticodon modifications and the corresponding deletion mutants of modifying enzymes tested in the study. **e**,**f**, The mcm^{5}s^2 modification does not make a difference in the varying SC-RT potential between the M and other forms of tRNA^{Gln}. The wt tRNA$^{Gln}_{UUG}$[L] (**e**) and mutant tRNA$^{Gln}_{U*UG}$[M] (**f**) isoacceptors were expressed individually (along with an EV) in wt and indicated mutant yeast cells and the efficiency of SC-RT on UAA-C was measured and evaluated as described in **b**,**c**; each bar is represented by $n \geq 5$ (**e**) and $n = 6$ (**f**) values.

least (UGA > UAG > UAA), as previously reviewed[35]. Therefore, we conclude that the impact of the stop codon identity per se is negligible and that the readthrough potential of tRNA$^{Gln}_{CUG}$[M] seems to lie predominantly in its primary sequence. In strong support, the reciprocal substitution of the anticodon from UUG to CUG in the tRNA$^{Gln}_{C*UG}$[L]$^{G42;G51;A66}$ mutant resulted in comparable levels of SC-RT on UAG, as in the case of the wt tRNA$^{Gln}_{UUG}$[L] on UAA (Fig. 1b,c).

For consistency, all tRNA constructs created in this study were flanked by the M isoacceptor untranslated regions (UTRs). Importantly, a direct comparison of all studied UUG isodecoders flanked by either genuine or M UTRs revealed no difference in their SC-RT-inducing potential (Extended Data Fig. 2). Northern blotting revealed that most of the tRNA^{Gln} variants used in this study were well expressed, as shown previously[19] and here (Extended Data Fig. 3a); only two tRNA^{Gln} variants did not reach elevated levels compared to the empty vector (EV), as explained below. Nonetheless, these control experiments ruled out that the observed differences were because of differing levels of individual tRNA variants and/or their integrity issues.

Importantly, while no information exists about modifications of the CUG anticodon and/or its adjacent nucleotides in the M isoacceptor[14], the UUG anticodon of all tRNA$^{Gln}_{UUG}$ isodecoders undergoes the 5-methoxycarbonylmethyl-2-thiouridine (mcm^{5}s^2) modification at U_{34} during the tRNA maturation process (Fig. 1d)[36]. Hence, we wondered whether this modification could compromise the SC-RT potential of the tRNA$^{Gln}_{UUG}$ isodecoders with the UUG anticodon sampling the UAA stop codon in the ribosomal A-site. Therefore, we expressed the tRNA$^{Gln}_{UUG}$[L] isodecoder in yeast strains individually deleted for genes required for the U_{34} modification (namely *ncs2Δ*, *ncs6Δ*, *elp2Δ* and *elp6Δ*; kindly provided by S. Leidel) (Fig. 1d). We assumed that, if mcm^{5}s^2 at U_{34} negatively influences SC-RT, we should record higher SC-RT values. On the contrary, for all four tested strains, the SC-RT efficiency of the wt tRNA$^{Gln}_{UUG}$[L] dropped to the EV background levels (Fig. 1e). Essentially the same effect was observed when the mutant tRNA$^{Gln}_{U*UG}$[M]$^{A42;A51;G66}$ isoacceptor was expressed in these deletion strains (Fig. 1f). Northern blotting revealed that neither of these deletions markedly impacted the expression levels of these two

tRNAs (Extended Data Fig. 3b). Please note that the northern probe was designed to fully match bases 43 through 72 of the $tRNA^{Gln}_{CUG}$[M] molecule. Therefore, the recognition specificity of $tRNA^{Gln}_{UUG}$[L] is reduced because of two internal mismatches at positions A66 and G51, which in turn magnifies the relative noise signal in the EV lanes observed in the experiment with $tRNA^{Gln}_{UUG}$[L] (upper three lanes) because this probe naturally recognizes all other native $tRNA^{Gln}_{UUG}$ isodecoders.

Collectively, these results, thus, not only correlate with the previous work[14] but also clearly suggest that it is not the modification of mcm^5s^2 that causes the differential SC-RT potential between the M form and all other forms of $tRNA^{Gln}$. On the contrary, it modestly promotes the misincorporation of the $tRNA^{Gln}_{UUG}$ isodecoders at the UAA stop codon. Therefore, we ruled out the impact of the anticodon and its modifications.

To test the effect of the $tRNA^{Gln}$ primary sequence, we individually or in various combinations substituted the bases of wt $tRNA^{Gln}_{CUG}[M]^{A42;A51;G66}$ at positions 42, 51 and 66 with those occurring in the L isoacceptor. While A51G increased SC-RT, G66A significantly decreased it and, strikingly, A42G displayed exactly the same effect as the triple mutation (in $tRNA^{Gln}_{CUG}[M]^{A42G;A51G;G66A}$), that is, the most pronounced decrease (Fig. 2a). Note that the triple mutant is, apart from the anticodon, fully identical to the $tRNA^{Gln}_{UUG}[L]^{G42;G51;A66}$ isoacceptor, resembling all other $tRNA^{Gln}_{UUG}$ isodecoders (Fig. 1a). Consequently, $tRNA^{Gln}_{CUG}[M]^{A42G;A51G;G66A}$ generates a weaker northern blot signal because of two internal mismatches with the northern probe used as described above (Extended Data Fig. 3a). Because the effect of the A42G;G66A double substitution practically mimicked that of A42G alone (Fig. 2a), we conclude that the A42 base is the major readthrough effector of the $tRNA^{Gln}_{CUG}$[M] isoacceptor. In agreement, the $tRNA^{Gln}_{UUG}$[E2] isodecoder that naturally carries adenine at position 42, in contrast to all other $tRNA^{Gln}_{UUG}$ isodecoders, showed the most efficient SC-RT among them (Fig. 1c).

Next, we reversed our approach and, instead of diminishing or eliminating the efficiency of SC-RT of the wt $tRNA^{Gln}_{CUG}[M]^{A42;A51;G66}$ isoacceptor by targeted substitutions (Fig. 2a), we took the wt $tRNA^{Gln}_{UUG}[L]^{G42;G51;A66}$ isodecoder with its natural UUG anticodon and attempted to boost its propensity for SC-RT with reciprocal substitutions at positions 42, 51 and 66. As can be seen in Fig. 2b, we obtained data inversely reflecting those shown in Fig. 2a. Altogether, these findings clearly illustrate that there are features in the backbone of the $tRNA^{Gln}_{CUG}$[M] isoacceptor, with the prevalent participation of A42 in its AS, that render this particular tRNA highly efficient in promoting SC-RT.

The 28:42 AS base pair the of $tRNA^{Gln}$[M] is crucial for SC-RT

Adenine 42 of the $tRNA^{Gln}_{CUG}$[M] isoacceptor base pairs with U28 in its AS (Fig. 1a). To investigate to what extent the Watson–Crick (W–C) base pairing in the 28:42 pair contributes to the efficiency of readthrough, we substituted bases at these positions with those either breaking base pairing or restoring it by different means. To the best of our knowledge, neither of these bases of this particular tRNA is subject to modifications[34,37]. Of note, position 28 is known to be modified by pseudouridine synthase Pus1 in several tRNAs but not in $tRNA^{Gln}$ (ref. 37). In agreement, deletion of *PUS1* had no effect on the efficiency of SC-RT of $tRNA^{Gln}_{CUG}$[M] in our previous experiments[19]. First, we tested the variant retaining the W–C base pairing but with U28:A42 swapped to create the U28A:A42U pair. Interestingly, its UAG-C SC-RT activity dropped ~3-fold (that is, to the same level as when the base pairing was broken by the key A42G substitution) (Fig. 2c). On the contrary, restoring the base paring of A42G by introducing the U28C substitution behaved as wt $tRNA^{Gln}_{CUG}$[M]. Swapping the U28C:A42G pair (that is, creating U28G:A42C), however, also led to a ~3-fold drop in the SC-RT efficiency, similarly to the case of the U28A:A42U swap (Fig. 2c). As expected, the pyrimidine:pyrimidine (U28:A42C) pair did not show elevated SC-RT levels (Fig. 2c). The purine:purine (U28G:A42 and U28A:A42) pairs displayed no measurable activity above the EV (Fig. 2c), indicating that these substitutions produce nonfunctional tRNAs. Consistently, northern blotting confirmed increased expression (compared to the EV) of all tRNAs but the latter $tRNA^{Gln}_{CUG}[M]^{U28G}$ (Extended Data Fig. 3a). The lower signal of $tRNA^{Gln}_{CUG}[M]^{A42G;A51G;G66A}$ is explained above. These results, thus, clearly demonstrate that, other than for purine:purine variants ($tRNA^{Gln}_{CUG}[M]^{U28G}$ and $tRNA^{Gln}_{CUG}[M]^{U28A}$), the overall integrity, charging and functionality of all other mutants are not affected because their activity never falls below the ~3-fold stimulation level of $tRNA^{Gln}_{C*UG}$[L] over the EV displayed in Fig. 1b. Taken together, our findings indicate that, in addition to the W–C base pairing of the 28:42 pair, pyrimidine is strongly preferred at position 28 and purine is strongly preferred at position 42 for the $tRNA^{Gln}_{CUG}$[M] isoacceptor to stimulate efficient SC-RT.

To further support the key role of this specific arrangement, we expressed the wt $tRNA^{Gln}_{CUG}$[M] isoacceptor and its purine:pyrimidine U28G:A42C mutant variant in *T. brucei*, where we recently established the SC-RT dual-lucifierase system and where the conserved effects of mutations affecting the length of the AS of $tRNA^{Trp}_{CCA}$ were initially observed[32]. Whereas wt $tRNA^{Gln}_{CUG}$[M] exhibited very efficient SC-RT even in this parasitic protist evolutionarily very distant from yeast, the U28G:A42C mutation completely eliminated it (Fig. 2d). Furthermore, *T. brucei* contains one gene encoding $tRNA^{Gln}_{UUG}$ and two genes encoding $tRNA^{Gln}_{CUG}$. All three observe the pyrimidine:purine rule with C28 and G42 and the latter isoacceptor promotes efficient SC-RT in *T. brucei* (Fig. 2e). While swapping C with G (in C28G:G42C) or disrupting the W–C base pairing by the C28U substitution completely eliminated the SC-RT potential of $tRNA^{Gln}_{CUG}$, substituting pyrimidine with pyrimidine and purine with purine (in C28U:G42A) preserved efficient readthrough (Fig. 2e). Northern blotting confirmed the stable expression of all tRNAs tested (Extended Data Fig. 3c). Overall, these results strongly suggest a general nature of preferential selection of $tRNA^{Gln}$ with pyrimidine 28 and purine 42 forming the fourth AS pair by the ribosome.

Genomic bias toward the 28:42 AS bp in ciliates

The ciliates (*Ciliophora*) are well known for their propensity to stop codon reassignments[38]. In several ciliate lineages, UAR stop codons occur within their coding sequences, being reassigned to encode glutamine. Functionally, these organisms require $tRNA^{Gln}$ to allow SC-RT on in-frame UAR codons for the synthesis of full-length proteins. Therefore, we asked whether there is a genomic bias in UAR-to-glutamine reassigned ciliates toward $tRNAs^{Gln}$-encoding genes with the fourth AS base pair observing the pyrimidine:purine 28:42 rule as described above, which allows for more efficient SC-RT. As shown in Extended Data Fig. 4 and Extended Data Table 1 and Supplementary Table 7 (details in Supplementary Information), we show here that it is indeed the case.

Interplay between $tRNA^{Gln}$[M] and factors modulating SC-RT

Previously, we and others showed that the identity of a nucleotide following the termination codon (position +4) defines a so-called stop codon tetranucleotide, which determines the preferences of rti-tRNAs for a given tetranucleotide[11,19]. Here, we show that there seems to be no functional interplay between the key tRNA backbone bases and the stop codon context including the key +4 base of the stop codon tetranucleotide (Fig. 3a,b; details in Supplementary Information).

Earlier, we also revealed that, in addition to its indispensable initiation roles[39], the multisubunit translation initiation complex eIF3 controls termination and critically promotes programmed SC-RT on all three stop codons[16,17,40]. Detailed analysis of the UGA and UAA stop codons and all near-cognate tRNAs suggested that eIF3 promotes incorporation of only those rti-tRNAs that have a mismatch at the third (wobble) position (that is, rti-$tRNA^{Trp}_{CCA}$ and rti-$tRNA^{Cys}_{GCA}$ for UGA and rti-$tRNA^{Tyr}_{GUA}$ for UAA). Here, we asked whether eIF3 also contributes to UAG SC-RT promoted by the $tRNA^{Gln}_{CUG}$[M] isoacceptor, which has a mismatch at the first position. Our results, presented in Fig. 4a

https://doi.org/10.1038/s41594-024-01450-z

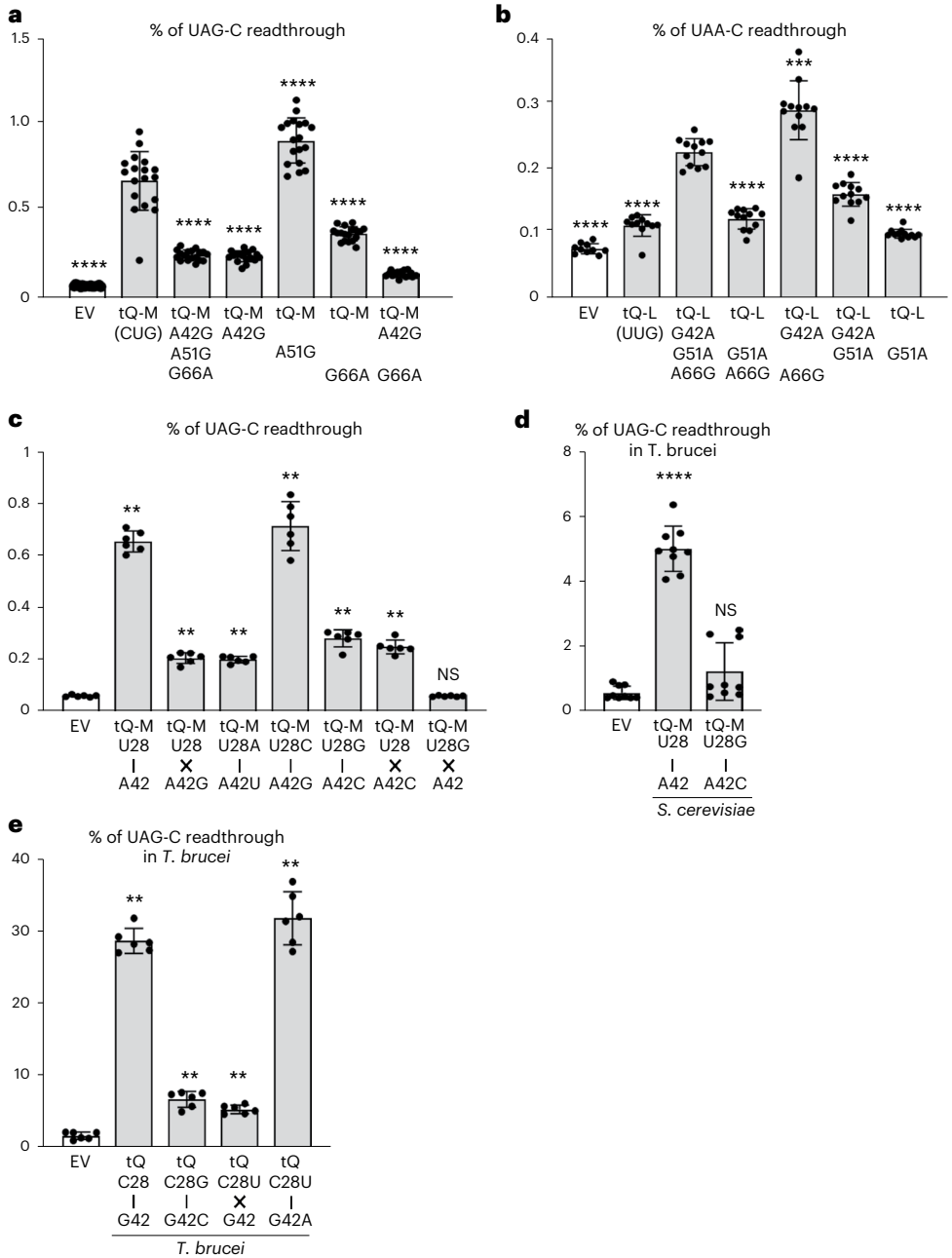

Fig. 2 | Primary sequence of tRNA^{Gln} determines the SC-RT efficiency. **a**,**b**, The wt and mutant CUG (**a**) and UUG (**b**) tRNA^{Gln} isoacceptors with indicated backbone substitutions were expressed individually (along with the EV) in wt yeast cells and the SC-RT efficiency on UAG-C (**a**) or UAA-C (**b**) was measured and evaluated as described in Fig. 1b,c; each bar is represented by $n \geq 17$ (**a**) or $n \geq 11$ (**b**) readthrough values. **c**, The nature of the AS 28:42 bp is critical for the increased propensity of the tRNA$^{Gln}_{CUG}$[M] isoacceptor for SC-RT. The wt and indicated mutant variants of tRNA$^{Gln}_{CUG}$[M] were expressed individually (along with the EV) in wt yeast cells and the SC-RT efficiency on UAG-C was measured and evaluated as described in Fig. 1b,c; each bar is represented by $n = 6$ values. The nature of hydrogen bonding between the 28:42 bp is indicated by a vertical black line (W–C base paring) or a black cross (no W–C paring). **d**, The wt and the A42G mutant of yeast tRNA$^{Gln}_{CUG}$[M] were expressed individually (along with the EV) in the procyclic forms of *T. brucei* bearing the dual-luciferase cassette with in-frame UAG-C. Transformed cells were processed for UAG readthrough measurements (Methods). Readthrough values were normalized to the control cell line values and evaluated as described in Fig. 1b,c; each bar is represented by $n = 9$ values. **e**, The wt and the indicated mutant variants of the *T. brucei* tRNA$^{Gln}_{CUG}$ were expressed individually (along with the EV) in the procyclic forms of *T. brucei* bearing the dual-luciferase cassette with in-frame UAG-C and processed as described in **d**; each bar is represented by $n = 9$ values.

(details in Supplementary Information), imply that eIF3 (1) greatly promotes SC-RT of all four rti-tRNAs (tRNA$^{Cys}_{GCA}$, tRNA$^{Trp}_{CCA}$, tRNA$^{Tyr}_{GUA}$ and tRNA$^{Gln}_{CUG}$[M]) regardless of whether the mismatch occurs at the first or third positions and (2) does not facilitate the ability of the tRNA$^{Gln}_{CUG}$[M] isoacceptor to markedly boost SC-RT.

Next, we examined the wt and mutant tRNA$^{Gln}_{CUG}$[M] in the background of the *sup45*^{Tyr410Ser} mutation of eRF1 (encoded by *SUP45*), which directly disrupts the eRF1–eRF3 interaction and, thus, weakens eRF1 binding to the A-site-situated stop codon, resulting in robust SC-RT[41]. We showed that reducing the A-site-binding affinity of eRF1, as the tRNA's major competitor for this site, did not mitigate differences between the wt and mutant tRNA$^{Gln}_{CUG}$[M] (Fig. 4b). This result clearly demonstrates that the difference in the propensity for SC-RT between M and other forms of tRNA^{Gln} does not originate from varying ability

https://doi.org/10.1038/s41594-024-01450-z

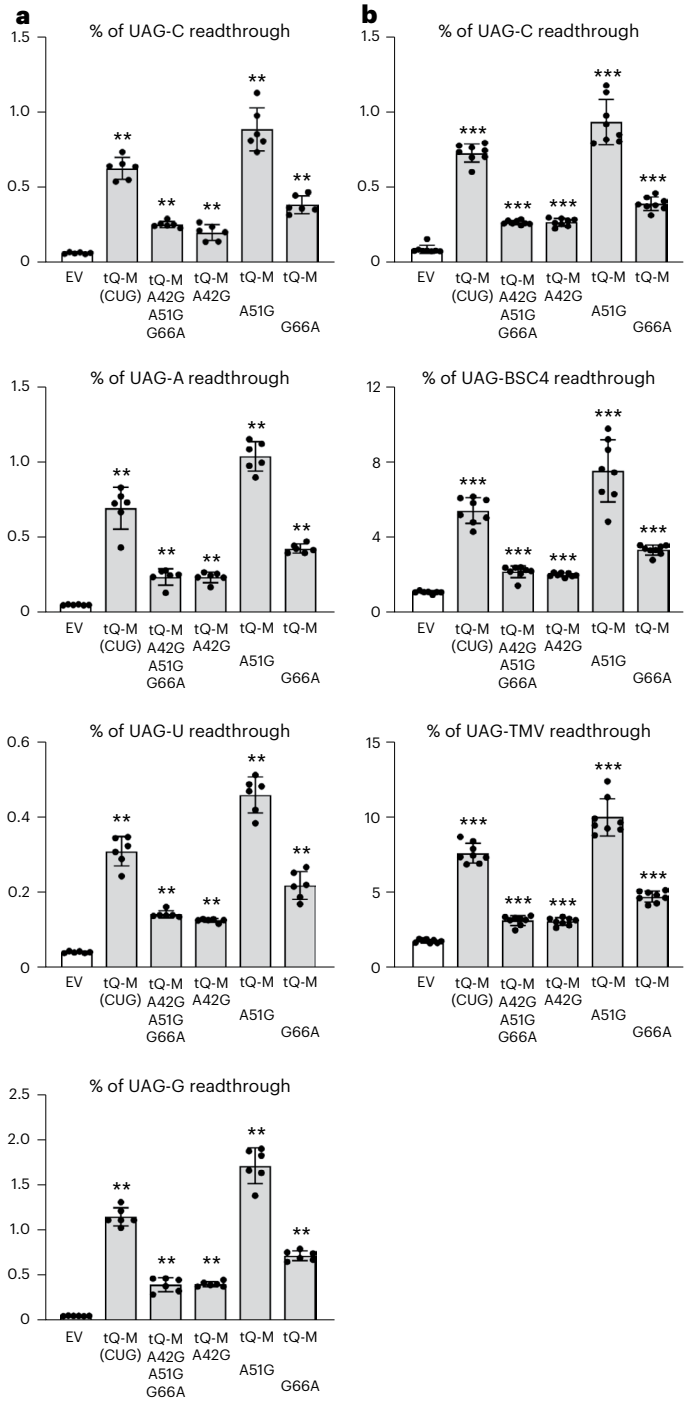

Fig. 3 | Stop codon context has no impact on the SC-RT efficiency of the tRNA$^{Gln}_{CUG}$[M] isoacceptor. a,**b**, The wt and mutant variants of the tRNA$^{Gln}_{CUG}$[M] isoacceptor with indicated backbone substitutions were expressed individually (along with the EV) in wt yeast cells and the efficiency of SC-RT on the UAG-N (**a**) or UAG-C, UAG-BSC4 and UAG-TMV (**b**) stop codon contexts was measured and evaluated as described in Fig. 1b,c; each bar is represented by $n = 6$ (**a**) and $n \geq 7$ (**b**) values.

of these tRNAs to outcompete eRF1 during stop codon recognition (details in Supplementary Information).

Paromomycin is a widely used drug for translation termination studies relaxing the A-site codon decoding pocket. Here, we show these paromomycin-induced changes, which prevent the ribosome from discriminating against near-cognate tRNAs, do not affect the stimulatory effect of the tRNA$^{Gln}_{CUG}$ backbone bases on SC-RT (Fig. 4c; details in Supplementary Information). Please also note that paromomycin concentration tested had no notable impact on cell viability (Fig. 4d). Where does this effect come from then?

Rps30/eS30 promotes tRNA^{Gln}[M] incorporation into the A-site

Next, we wondered whether the tRNA backbone bases establish direct interactions with the A-site ribosomal components outside of the codon decoding pocket to facilitate the codon sampling and/or accommodation processes. Previous reports suggested that the aa-tRNA interacts with h18 and h30 of 18S rRNA and small ribosomal proteins Rps23/uS12, Rps15/uS19, Rps25/eS25, Rps30/eS30 and/or Rps31/eS31 (refs. 24,29–31). On the basis of the available data and Protein Data Bank (PDB) searches, we focused on the latter three proteins because their flexible domains could stretch out to contact the AS 28:42 base pair (Fig. 5a). Please note that the tRNA model shown in this figure (based on *Escherichia coli* tRNA^{Lys}) represents a mixture of tRNAs and is only used for illustration purposes; it does not represent tRNA^{Gln}. In particular, we inspected the N terminus of Rps30/eS30, the C terminus of Rps15/uS19 and/or the N terminus of Rps25/eS25 (refs. 24,29,30). According to the available literature, the most intriguing contacts could be mediated by the first five extreme N-terminal residues and Arg10 of Rps30/eS30 (refs. 24,29). To test the prospective role of Rps30/eS30 in facilitating the tRNA$^{Gln}_{CUG}$[M] accommodation in the A-site, we generated several site-specific substitutions of the first ten N-terminal residues of Rps30/eS30 tagged with a FLAG tag at its C terminus and expressed them in a yeast *rps30a*;*rps30b* double deletion strain. None of the mutants displayed a severe growth phenotype at any tested temperatures (Fig. 5b). Interestingly, whereas *rps30b*$^{\Delta 2-6}$–FLAG, *rps30b*^{5Ala10}–FLAG, *rps30b*^{Lys3Gly}–FLAG and *rps30b*^{His5Gly}–FLAG mutants robustly decreased SC-RT on UAG-BSC4, *rps30b*^{Ala2Gly}–FLAG and *rps30b*^{Val4Ala}–FLAG increased it, while *rps30b*^{Arg10Ala}–FLAG had a minimal effect (Fig. 5c). Similar results were obtained with UAA-BSC4 and UGA-BSC4 stop codons (Extended Data Fig. 5a,b). The robustness of the increase in SC-RT induced by *rps30b*^{Val4Ala}–FLAG exclusively on UAA and the significant decrease in SC-RT induced by *rps30b*^{Arg10Ala}–FLAG exclusively on UGA are discussed below. Altogether, these results clearly implicate the N terminus of Rps30/eS30 in controlling the stop codon decoding process.

Next, we individually expressed wt and mutant forms of the tRNA$^{Gln}_{CUG}$[M] isoacceptor in Rps30/eS30 wt and mutant strains. Except for Arg10Ala (Fig. 5d and Extended Data Fig. 6a), none of the Rps30/eS30 substitutions displayed any interaction with tRNA$^{Gln}_{CUG}$[M] mutants (Extended Data Fig. 6b). Intriguingly, the Arg10Ala substitution dramatically reduced the SC-RT-inducing potential of the wt tRNA$^{Gln}_{CUG}$[M] isoacceptor when compared to the EV control and to the A42G mutants in both tested stop codon contexts (Fig. 5d and Extended Data Fig. 6a). Importantly, the SC-RT-inducing potential of another UAG rti-tRNA (namely tRNA$^{Tyr}_{GUA}$) was not affected at all by *rps30*^{Arg10Ala} (Fig. 5d and Extended Data Fig. 6a). Please note that the *rps30b*^{Arg10Ala}–FLAG mutant affected neither the polysome content nor the 60S:40S ratio (Extended Data Fig. 7a,b). Also note that the reason for the overall lower SC-RT values obtained with wt tRNA$^{Gln}_{CUG}$[M] (Fig. 5d and Extended Data Fig. 6a versus, for example, Fig. 1b) is a different genetic background that was used to delete both copies of RPS30-encoding genes.

Finally, we reversed the charge in the Arg10Asp mutant and observed that it completely eliminated the ability of tRNA$^{Gln}_{CUG}$[M] to promote SC-RT (Fig. 5e). At the same time, the Arg10Lys substitution retaining the positive charge had no specific impact on the stop-codon-promoting activity of tRNA$^{Gln}_{CUG}$[M] or its A42G mutant variant (Fig. 5e). In other words, the fold increases in wt (~3-fold) and mutant (~1.5-fold) tRNA$^{Gln}_{CUG}$[M] remained virtually the same in both wt and Arg10Lys mutant cells. Strikingly, however, the Arg10Lys substitution increased overall SC-RT ~5–6-fold in all three strains tested (that is,

https://doi.org/10.1038/s41594-024-01450-z

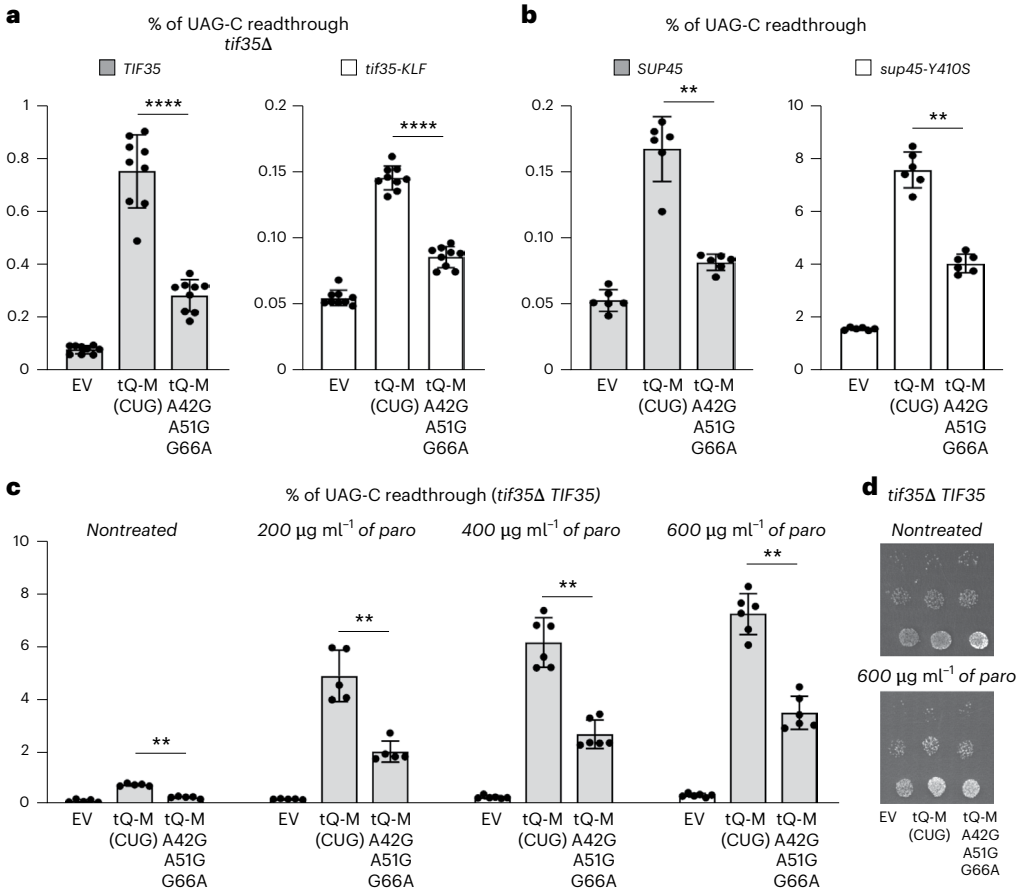

Fig. 4 | Interplay between tRNA^{Gln}[M] and factors modulating SC-RT. a, eIF3 does not influence the SC-RT efficiency of tRNA$^{Gln}_{CUG}$[M]. The wt and mutant variant of tRNA$^{Gln}_{CUG}$[M] with indicated backbone substitutions were expressed individually (along with the EV) in wt and *tif35-KLF* mutant yeast cells and the SC-RT efficiency on UAG-C was measured and evaluated as described in Fig. 1b,c; each bar is represented by $n = 9$ values. **b**, Disrupting the eRF1–eRF3 interaction by a specific mutation of eRF1 does not influence the SC-RT efficiency of tRNA$^{Gln}_{CUG}$[M]. The wt and a mutant variant of tRNA$^{Gln}_{CUG}$[M] with indicated backbone substitutions were expressed individually (along with the EV) in wt and *sup45*^{Tyr410Ser} mutant yeast cells and the SC-RT efficiency on UAG-C was measured and evaluated as described in Fig. 1b,c; each bar is represented by $n = 6$ values. **c**, Paromomycin does not influence the SC-RT efficiency of tRNA$^{Gln}_{CUG}$[M]. The wt and a mutant variant of the tRNA$^{Gln}_{CUG}$[M] isoacceptor with indicated backbone substitutions were expressed individually (along with the EV) in wt yeast cells in the presence of varying paromomycin concentrations and the SC-RT efficiency on UAG-C was measured and evaluated as described in Fig. 1b,c; each bar is represented by $n \geq 5$ values. **d**, Growth rate analysis of the wt cells expressing either EV or wt or a mutant variant of tRNA$^{Gln}_{CUG}$[M] upon paromomycin treatment; cells were spotted in three serial tenfold dilutions on YPD medium with or without paromomycin and incubated for 3 days at 30 °C.

irrespective of the A42G mutation). The Arg10Lys cells expressing wt tRNA$^{Gln}_{CUG}$[M] exhibited an ~18-fold increase over the wt strain expressing EV; that is, a multiplicative increase in individual increases (~6-fold for Arg10Lys alone times ~3-fold for tRNA$^{Gln}_{CUG}$[M] alone) was observed. This suggests that lysine in the place of Arg10 generally reduces the fidelity of stop codon recognition while preserving the ability of wt tRNA$^{Gln}_{CUG}$[M] to act as highly efficient rti-tRNA. Note that, despite these effects, only the Arg10Asp substitution led to a mild slow growth phenotype (Fig. 5f).

Taken together, these findings strongly support the view that Arg10 of Rps30/eS30, most probably because of its positive charge, potentiates the SC-RT ability of tRNA$^{Gln}_{CUG}$[M] by directly contacting the 28:42 base pair of its AS.

Interactions of A-site riboproteins with rti-tRNAs drive SC-RT

We recently discovered that shortening the AS of *S. cerevisiae* tRNA$^{Trp}_{CCA}$ from canonical 5 bp to 4 bp, while preserving its overall length, robustly (~7-fold) increased the SC-RT potential of the shorter AS tRNA variant[32]. Remarkably, this 'short AS' tRNA$^{Trp}_{CCA}$ naturally occurs in a handful of eukaryotes with all stop codons reassigned to sense codons[32]. Thus, together with the tRNA$^{Gln}_{CUG}$[M] described here, we found two cases of naturally occurring tRNA variants with markedly increased SC-RT potential compared to other variants encoding the same amino acids. This may suggest that it is the extra noncovalent interactions between the tRNA backbone and the A-site components, as demonstrated here for tRNA^{Gln}, which generally confer all rti-tRNAs the advantage of increased SC-RT over other near-cognate tRNAs. To test that, we subjected the aforementioned C terminus of Rps15/uS19 and the N terminus of Rps25/eS25 (both projecting into the A-site[30,31]) to a thorough mutagenesis. Subsequently, we examined the effect of the resulting mutants, together with all our Rps30/eS30 mutants, on the propensity of all four rti-tRNAs to increase SC-RT on corresponding stop codons in a complex approach.

While the Arg10Ala substitution significantly reduced (by ~30%) the SC-RT potential of the 5-bp-long AS tRNA$^{Trp}_{CCA}$, as in the case of the EV control (Fig. 6a, second and sixth bars), the 4-bp-long AS variant with much higher SC-RT became resistant to this reduction (Fig. 6a, sixth versus tenth bar). These results further support the idea that Arg10 of eS30 can somehow monitor the geometry of the AS unless it is disturbed by substitutions changing the nature of the AS bases or its length. In contrast, neither Ala2Gly nor Val4Ala substitutions of Rps30/eS30 showed any effect with any length variant of tRNA$^{Trp}_{CCA}$ (Fig. 6a). Neither these substitutions nor, importantly, the Arg10Ala substitution affected the SC-RT potential of tRNA$^{Tyr}_{GUA}$, whose fourth

https://doi.org/10.1038/s41594-024-01450-z

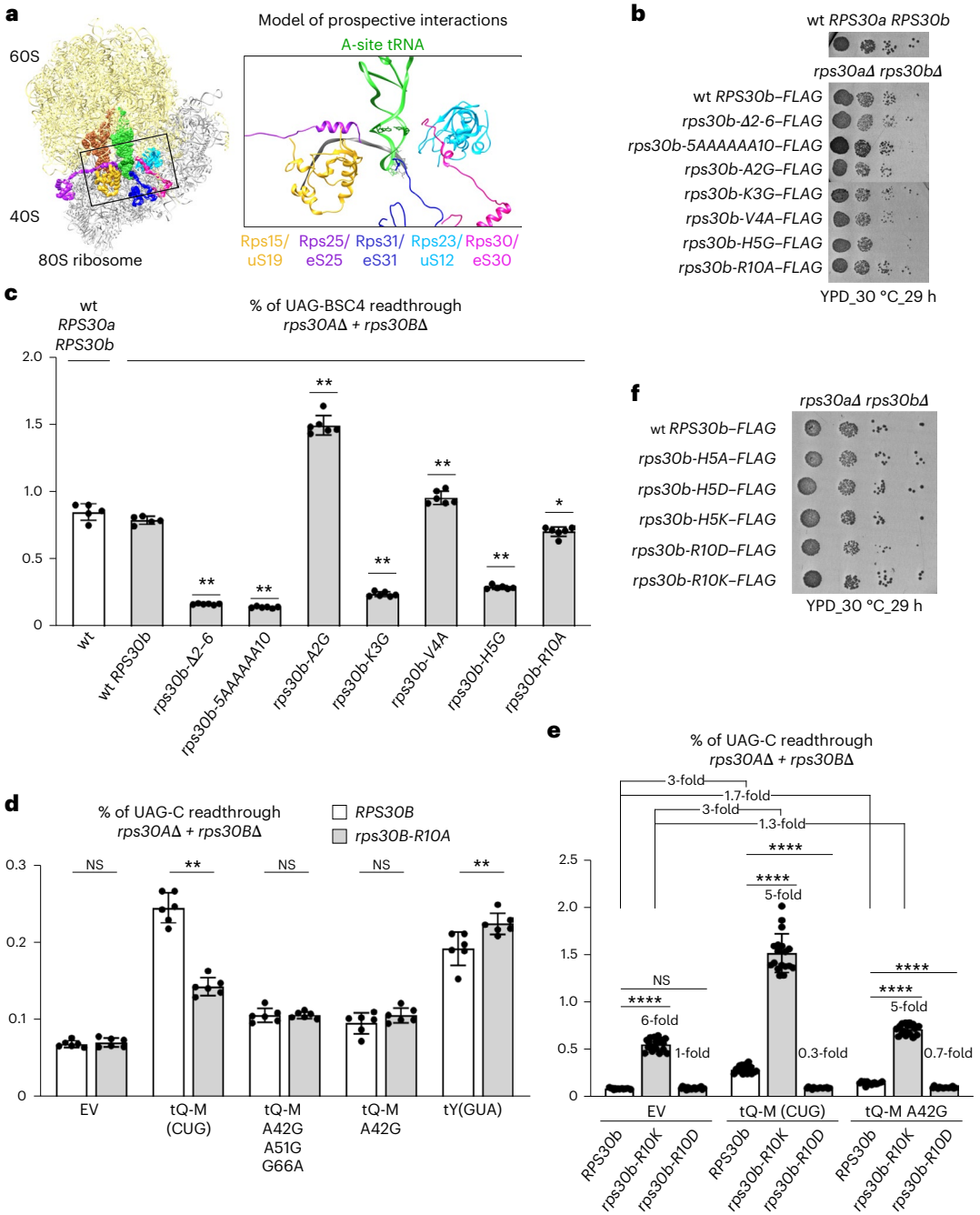

Fig. 5 | Rps30/eS30 promotes tRNA^{Gln}[M] incorporation into the A-site. **a**, Left, the yeast 80S ribosome shown from the top (PDB 7RR5); right, zoomed-in view to highlight the A-site. Shown are prospective contacts between the tRNA AS and ribosomal proteins. The 28:42 base pair is depicted in dark green with spheres (left) or sticks (right). The terminal tails of highlighted ribosomal proteins are known to be flexible and the exact positions and length of fitted amino acids vary between different structures. The terminal amino acids fitted are Gly129 of Rps15/uS19, Gln6 of Rps25/eS25, Arg4 of Rps31/eS31, full-length Rps23/uS12 and Ala2 of Rps30/eS30. **b**, Growth rate analysis of the N-terminal substitution mutants of Rps30/eS30. **c**, Rps30/eS30 mutants differentially modulate the SC-RT efficiency on UAG. The wt and indicated Rps30/eS30 mutant yeast cells were tested for the SC-RT efficiency in the UAG-BSC4 stop codon context as described in Fig. 1b,c; each bar is represented by $n \geq 5$ values. **d**, Arg10 of Rps30/eS30 potentiates the SC-RT-promoting ability of tRNA$^{Gln}_{CUG}$[M] by directly contacting the AS 28:42 base pair. The wt and indicated mutant variants of tRNA$^{Gln}_{CUG}$[M] and control tRNA$^{Tyr}_{GUA}$ were expressed individually (along with the EV) in wt and *rps30B*^{R10A} mutant yeast cells and the SC-RT efficiency on UAG-C was measured and evaluated as described in Fig. 1b,c; each bar is represented by $n = 6$ values. **e**, The Arg10Asp substitution of Rps30/eS30 eliminates the SC-RT-promoting ability of tRNA$^{Gln}_{CUG}$[M], while the Arg10Lys substitution generally reduces termination fidelity. The wt and A42G mutant variants of tRNA$^{Gln}_{CUG}$[M] were expressed individually (along with the EV) in wt and *rps30B*^{Arg10Lys} or *rps30B*^{Arg10Asp} mutant yeast cells and the SC-RT efficiency on UAG-C was measured and evaluated as described in Fig. 1b,c; each bar is represented by $n \geq 16$ values. **f**, Growth rate analysis of the N-terminal substitution mutants of Rps30/eS30.

base pair does not obey the pyrimidine:purine rule (it has A:U at this position) (Fig. 5d and Extended Data Fig. 6). The $tRNA^{Tyr}_{GUA}$, thus, serves as a critical specificity control.

In the case of $tRNA^{Cys}_{GCA}$, Arg10Ala reduced its SC-RT potential twofold (Fig. 6b, second versus sixth bar). His5Gly, as the only other Rps30/eS30 substitution, then reduced the SC-RT potential of $tRNA^{Cys}_{GCA}$ even further (threefold; Fig. 6b, fourth versus eighth bar). Unexpectedly, substituting basic His5 for aspartic acid had no effect, whereas replacing His5 with basic lysine (or hydrophobic alanine) displayed a similar phenotype to that of the His5Gly mutant (that is, twofold reduction; Fig. 6c, second versus fifth bar). At present, we have no explanation for these observations.

Remarkably, the fourth base pair of wt $tRNA^{Cys}_{GCA}$ obeys the pyrimidine:purine rule (C:G). When we disrupted its W–C character with the C27U:G41 mutation, the SC-RT-promoting activity of mutant $tRNA^{Cys}_{GCA}{}^{C27U}$ became virtually insensitive to the Arg10Ala substitution of Rps30/eS30 (Fig. 6d). In detail, the threefold reduction seen between the EV control and wt $tRNA^{Cys}_{GCA}$ in the Arg10Ala mutant strain (0.6-fold versus 0.2-fold; second versus fourth bar) was nullified by the C27U:G41 mutation (second and fourth bars versus sixth bar (0.7-fold)). Together, we propose that the N terminus of Rps30/eS30, specifically Arg10 and His5, contacts the top of the AS of $tRNA^{Gln}_{CUG}$[M], $tRNA^{Trp}_{CCA}$ and $tRNA^{Cys}_{GCA}$ to facilitate their accommodation in the A-site.

While substitutions of Rps30/eS30 residues had no effect on the SC-RT potential of $tRNA^{Tyr}_{GUA}$, a fully viable double deletion of both Rps25/eS25-encoding genes (*RPS25A* and RPS25*B*), as well as a deletion of the 12 N-terminal amino acids in $rps25^{\Delta 2-13}$ expressed as a sole allele nearly eliminated its SC-RT potential (Fig. 7a,c). At the same time, however, both mutants had a minimal effect on the SC-RT efficiency of other three rti-tRNAs (Fig. 7a–c). In detail, the loss of Rps25/eS25 (Fig. 7a, top; first versus fourth bar) or only its extreme N terminus (Fig. 7c, first versus fourth bar) dramatically increased the fidelity of termination and, thus, in turn decreased the efficiency of SC-RT. Despite this overall decrease, the SC-RT efficiency commonly exhibited by $tRNA^{Cys}_{GCA}$ or $tRNA^{Trp}_{CCA}$ (irrespective of its AS length) was unchanged (Fig. 7a, bottom, b) and even increased 2–2.5-fold in the case of $tRNA^{Gln}_{CUG}$[M] (Fig. 7a, top, fifth versus second bar, 7c, fifth versus second bar). The opposite was true for $tRNA^{Tyr}_{GUA}$, whose SC-RT potential was reduced from fivefold to threefold in the Rps25/eS25 double deletion strain (Fig. 7a, top; third versus sixth bar) and from fourfold to twofold in the $rps25^{\Delta 2-13}$ mutant strain (Fig. 7c, top; third versus sixth bar). These findings indicate that the N terminus of Rps25/eS25 most probably contacts specifically $tRNA^{Tyr}_{GUA}$ to achieve its increased stabilization in the A-site, as in case of Rps30/eS30 and the other three rti-tRNAs.

Lastly, robust mutational analysis of Rps15/uS19 revealed only two mutants with markedly increased SC-RT potential: $rps15^{Arg130Ala}$ and $rps15^{128Ala134}$ (Extended Data Fig. 8a). However, we did not observe any specific interactions with either of the rti-tRNAs or their mutants (Extended Data Fig. 8b,c).

Discussion

In most noncanonical genetic codes, the UAG and UAA stop codons share near-cognate tRNAs delivering the same amino acids[42], which differ from those recognizing the UGA stop codon. In agreement with the genetic code standardly allowing wobble decoding of the third codon base and a well-documented tolerance for the first-base wobble decoding during recoding events, glutamine, tyrosine and lysine are incorporated during UAR readthrough, whereas arginine, cysteine and tryptophan are incorporated during UGA readthrough[18,21]. The efficiency of their incorporation depends on many factors, one of which is the cellular level that may vary from tissue to tissue. Nonetheless, when the relevant tRNAs were expressed individually to similar levels in *S. cerevisiae*, only four of them stood out as very potent facilitators of SC-RT, namely glutamine, cysteine, tyrosine and tryptophan[19]. Of note, the latter three were tested in human cell lines with similar results[20,43]. Why only these four?

Here and elsewhere[32], we demonstrated that, at least for $tRNA^{Gln}_{CUG}$[M], $tRNA^{Trp}_{CCA}$ and $tRNA^{Cys}_{GCA}$, the answer lies surprisingly not in the bases of their anticodon loop and/or their modifications but in their AS. In case of $tRNA^{Gln}_{CUG}$[M], the nature of the 28:42 anticodon base pair is sensed by the Arg10 of Rps30/eS30, whose substitution to Ala greatly mitigates the ability of $tRNA^{Gln}_{CUG}$[M] to promote efficient SC-RT on UAG, as does the alteration of the pyrimidine:purine character of its 28:42 base pair (Figs. 2 and 5d). Given that the Arg10Asp and Arg10Lys substitutions completely abolished or left intact the SC-RT-inducing potential of wt $tRNA^{Gln}_{CUG}$[M], respectively (Fig. 5e), we propose that the positive charge could by a major factor in this genetic interaction, as it may enable a direct ionic bond with a negatively charged 28:42 base pair.

In analogy, Arg10Ala and the His5 substitutions to glycine, lysine or alanine reduced the SC-RT potential of wt $tRNA^{Cys}_{GCA}$, which also obeys the pyrimidine:purine 28:42 rule. Because we obtained fully consistent data with wt and mutant variants of *S. cerevisiae* $tRNA^{Gln}_{CUG}$[M] and *T. brucei* $tRNA^{Gln}_{CUG}$ (Fig. 2d,e), we conclude that the importance of the pyrimidine:purine nature of the fourth AS base pair of at least these two rti-tRNAs (that is, $tRNA^{Gln}_{CUG}$[M] and $tRNA^{Cys}_{GCA}$) is evolutionary conserved. Notably, the importance of the top two AS pairs (fourth and fifth) of rti-tRNAs for SC-RT that we discovered here and elsewhere[32] also finds strong support in earlier work. Working with the *E. coli* $tRNA^{Trp}_{CCA}$ with the artificial GUC anticodon complementary to the glutamic acid codon CAG, it was shown that mutations disrupting base paring between G27 and A43 (that is, the bases forming the fifth pair of its AS) turned this tRNA into a potent synthetic suppressor permitting SC-RT at UAG[44]. Similarly, shortening of the AS of $tRNA^{Trp}_{CCA}$ from *S. cerevisiae* and *T. brucei* from 5 to 4 bp, while preserving the identity of their anticodon, dramatically boosted SC-RT at UAG[32].

Among the Rps30/eS30 N-terminal residues, mainly the basic Arg10 residue seems to monitor the length and proper base pairing of the AS, because its Ala substitution also genetically interacted with $tRNA^{Trp}_{CCA}$ and $tRNA^{Cys}_{GCA}$ and their mutant variants. In addition, while Rps30/eS30 mutants displayed no genetic interaction with $tRNA^{Tyr}_{GUA}$, Rps25/eS25 deletion or truncation of its N-terminal residues specifically prevented $tRNA^{Tyr}_{GUA}$ from stimulating SC-RT. These results, thus, further support the view that the architectures of individual tRNAs are well optimized[45]. However, this kind of natural fine-tuning not only compensates for the known destabilizing effect of certain amino acids that are bound to them. It also seems to ensure that specific contacts are made between the residues of the A-site ribosomal proteins and backbone bases of any tRNA to promote cognate codon–anticodon base pairing while preventing tRNA misincorporation at noncognate codons. In the case of rti-tRNAs, these contacts then increase their odds to be selected during SC-RT (Fig. 7d), as we demonstrated here. Indeed, when the sequence diversity among isodecoder tRNA genes was subjected to robust suppression analysis, it was concluded that the large difference in their suppression efficiency could not be explained solely by differences in tRNA folding because of their varying sequences but also by contacts they may establish with ribosomal components[46].

In particular, it was proposed that Rps30/eS30 may enhance the stability of a correct codon–anticodon interaction through its contact with the anticodon loop[24]. In the presence of a cognate aa-tRNA, the N terminus of Rps30/eS30 becomes ordered, allowing a conserved histidine (His76, corresponding to yeast His5 studied here) to reach into a groove between the phosphate backbone of the anticodon +1 position and the two flipped-out decoding bases to form potentially stabilizing contacts. In addition, it was suggested that, because this groove depends on the flipped nucleotides that accompany canonical codon–anticodon base pairing, Rps30/eS30 may preferentially stabilize cognate tRNAs to enhance discrimination[24]. Because our data strongly indicate that yeast His5 and Arg10 preferentially promote incorporation of a selected set of the nc-tRNAs into the A-site, it seems that eS30 may have a dual role. This could stabilize cognate tRNAs to enhance tRNA discrimination during kinetic proofreading of

https://doi.org/10.1038/s41594-024-01450-z

the initial selection and/or accommodation, while stabilizing certain near-cognate tRNAs at the A-site to increase their odds of being selected (Fig. 7d). Intuitively, for this specific class of tRNAs, the discriminatory role of eS30 would have to be suppressed.

In agreement with our results clearly indicating that the key AS base pair recognized by Arg10 is a purine 42 (or equivalent) base pairing with a pyrimidine 28 (or equivalent) of selected rti-tRNAs, all available structures of decoding complexes indicate that His5 and Arg10 (or the corresponding conserved residues in other organisms) could be positioned close to the AS of the A/T-state tRNA[24,29,47] (Extended Data Fig. 8d). The key unanswered question is how these two residues can read out characteristic structural features (for example, the fourth pyrimidine:purine 28:42 base pair) of the AS of some rti-tRNAs. One of our current ideas is presented in the Supplementary Information but further studies, for example, using cryo-electron microscopy of readthrough complexes, will be needed to provide the ultimate answer.

Interestingly, while only a mild increase in SC-RT was observed for the *rps30*^{Val4Ala} substitution on UAG and UGA, a very strong increase (~4-fold) was observed on UAA; similarly, while virtually no effect was observed for the *rps30*^{Arg10Ala} substitution on UAA and UAG, a notable drop in SC-RT (by ~30–50%) was observed on UGA (Fig. 5c and Extended Data Fig. 5). Strikingly, an extreme N-terminal residue Arg8 of human Rps30/eS30, corresponding to *S. cerevisiae* Arg10 studied here, was directly crosslinked to the +4 position of the mRNA (where the +1 position is the first nucleotide of the stop codon in the A-site) in a pretermination ribosome[48]. This is the base shown to be accommodated in the eukaryotic-specific U-turn-like conformation of the stop codon in the decoding pocket, which is formed when the N-terminal domain (NTD) of eRF1 contacts the ribosome[49,50]. It is also the base that has a notable impact on the efficiency of SC-RT[2,8–11]. In addition, the N-terminal tail of Rps30/eS30 is, along with Rps31/eS31 and several 18S rRNA sites, known to interact with the eRF1 NTD[51]. In fact, it is believed that, upon eRF1 binding, the N-terminal tail of Rps30/eS30 is shielded by the eRF1 NTD from interacting with the backbone of the stop codon as observed in a pretermination ribosome free of eRFs[48]. Thus, we propose that Rps30/eS30, through its N terminus, not only discriminates between individual tRNAs but also somehow recognizes the identity of a stop codon to facilitate its recognition by eRF1, thereby controlling the balance between translation termination and SC-RT.

In addition to Rps30/eS30, the AS of the A-site aa-tRNA appears to be in contact with the 12–15 C-terminal residues of Rps15/uS19, depending on the species. In addition, this region makes electrostatic interactions with the P-site tRNA, the rRNA helices h44 and h69 and the +4 position of the mRNA (for example, Arg8 (Arg10 in *S. cerevisiae*) of Rps30/eS30)[24,48,52]. However, we found no interactions between the C-terminal substitutions of this ribosomal protein and any of rti-tRNAs. This can be explained by two previous observations. Analysis of tRNAs associated with 40S subunits and 80S ribosomes showed that the

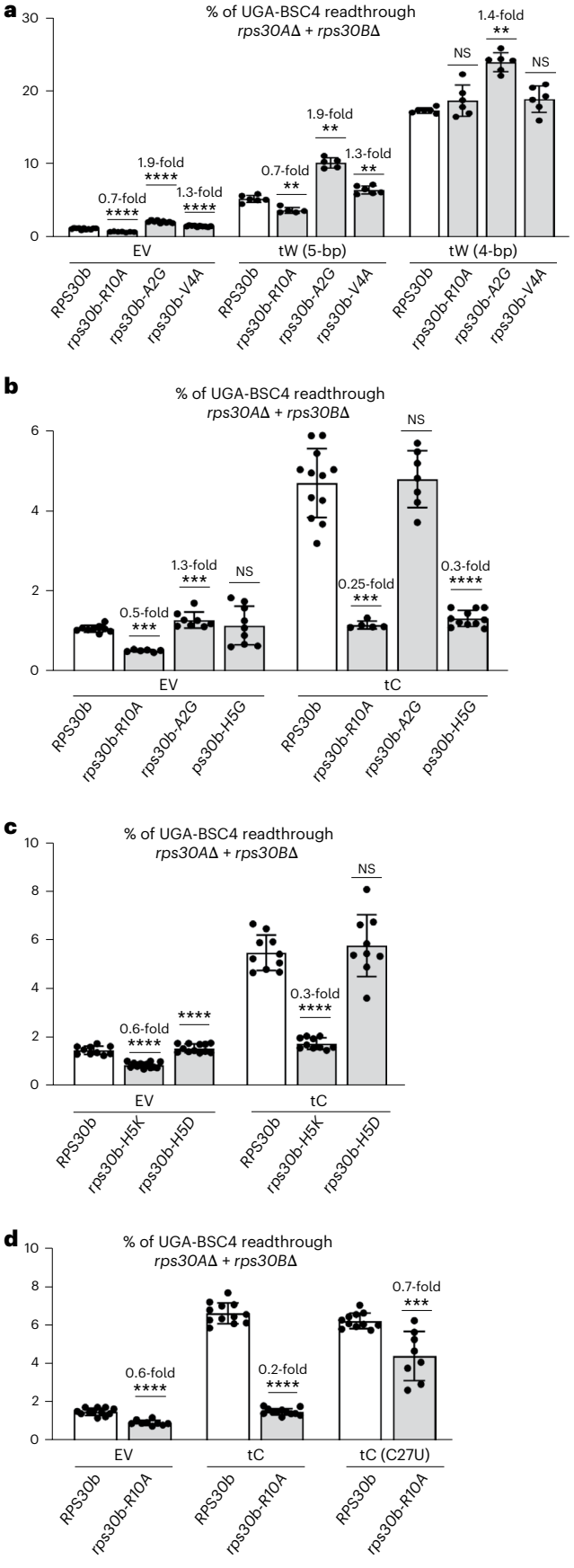

Fig. 6 | Arg10 of Rps30/eS30 ensures A-site incorporation of rti-tRNAs with the well-defined identity of the 28:42 base pair. a, Arg10 of Rps30/eS30 potentiates the SC-RT ability of wt tRNA$^{Trp}_{CCA}$ (with the 5-bp-long AS) while having no influence over its 4-bp-long mutant variant. The wt and a mutant variant of tRNA$^{Trp}_{CCA}$ were expressed individually (along with the EV) in wt and indicated *rps30B* mutant yeast cells and the SC-RT efficiency on UAG-BSC4 was measured and evaluated as described in Fig. 1b,c; each bar is represented by $n \geq 5$ values. **b**, His5 and Arg10 of Rps30/eS30 potentiate the SC-RT ability of tRNA$^{Cys}_{GCA}$. The wt tRNA$^{Cys}_{GCA}$ was expressed (along with the EV) in wt and indicated *rps30B* mutant yeast cells and the SC-RT efficiency on UGA-BSC4 was measured and evaluated as described in Fig. 1b,c; each bar is represented by $n \geq 5$ values. **c**, Substituting His5 of Rps30/eS30 for lysine or aspartic acid shows varying effects on the SC-RT-promoting ability of tRNA$^{Gln}_{CUG}$[M]. The wt tRNA$^{Cys}_{GCA}$ was expressed (along with the EV) in wt and indicated *rps30B* mutant yeast cells and the SC-RT efficiency on UGA-BSC4 was measured and evaluated as described in Fig. 1b,c; each bar is represented by $n \geq 10$ values. **d**, Mutant tRNA$^{Cys}_{GCA}$ (C28U:G42) becomes insensitive to the Arg10Ala substitution of Rps30/eS30. The wt and mutant tRNA$^{Cys}_{GCA}$ were expressed (along with the EV) in wt and the Arg10Ala mutant of Rps30/eS30 and the SC-RT efficiency on UGA-BSC4 was measured and evaluated as described in Fig. 1b,c; each bar is represented by $n \geq 8$ values.

https://doi.org/10.1038/s41594-024-01450-z

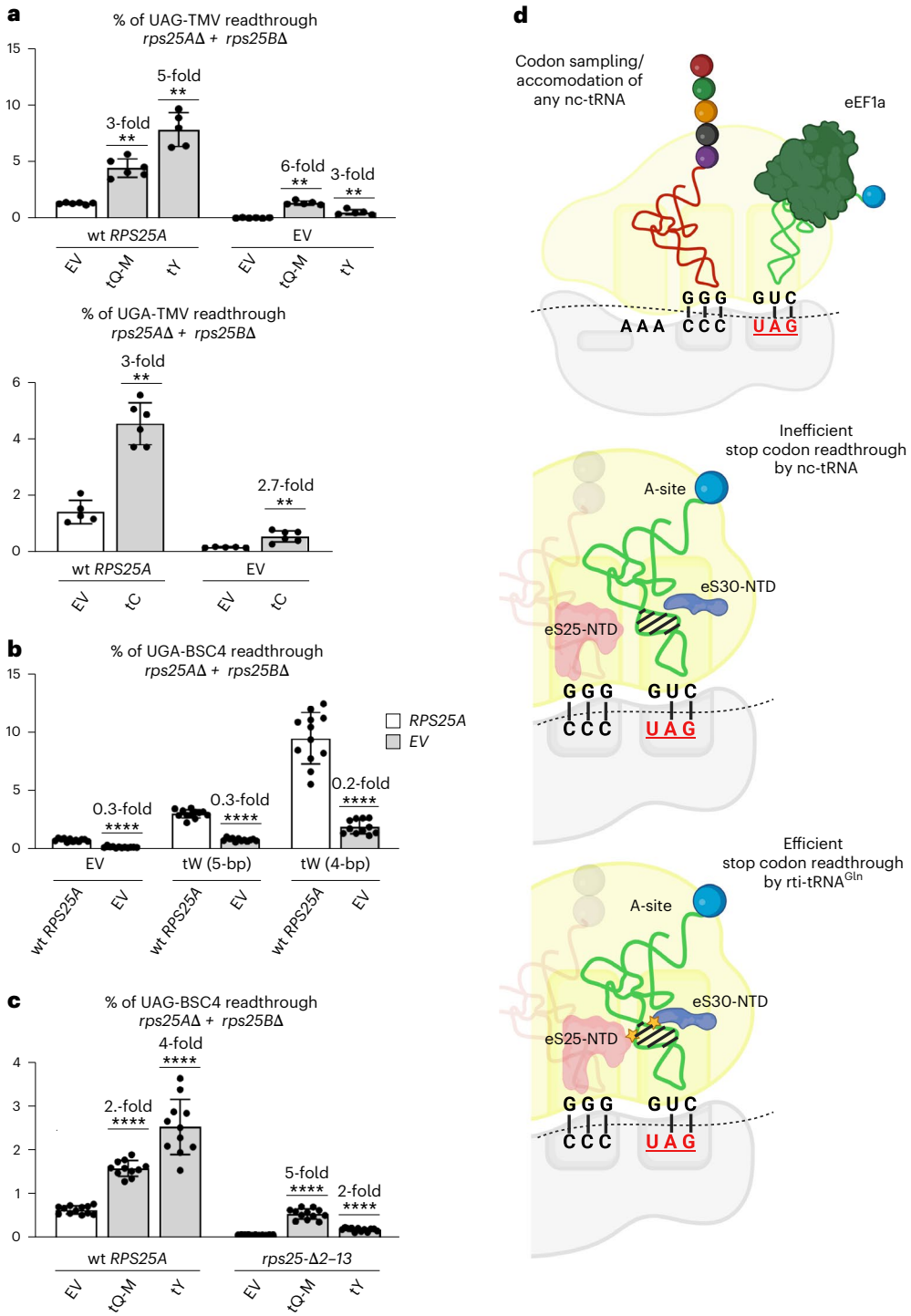

Fig. 7 | The Rps25/eS25 N-terminal residues promote incorporation of rti-tRNA$^{Tyr}_{GUA}$ into the ribosomal A-site. a, Loss of Rps25/eS25 protein diminishes the SC-RT ability of tRNA$^{Tyr}_{GUA}$ as the only rti-tRNA. The wt tRNA$^{Gln}_{CUG}$[M], tRNA$^{Tyr}_{GUA}$ and tRNA$^{Cys}_{GCA}$ rti-tRNAs were expressed individually (along with the EV) in wt and *rps25A*;*rps25B* double deletion cells and the SC-RT efficiency on corresponding stop codons was measured and evaluated as described in Fig. 1b,c; each bar is represented by $n \geq 5$ values. **b**, Loss of Rps25/eS25 protein has no influence over the SC-RT potential of wt and mutant tRNA$^{Trp}_{CCA}$. The wt and a mutant variant of tRNA$^{Trp}_{CCA}$ were expressed individually (along with the EV) in wt and *rps25A*;*rps25B* double deletion cells and the SC-RT efficiency on UGA-BSC4 was measured and evaluated as described in Fig. 1b,c; each bar is represented by $n \geq 11$ values. **c**, The N-terminal Rps25/eS25 residues promote incorporation of the rti-tRNA$^{Tyr}_{GUA}$ into the ribosomal A-site. The wt tRNA$^{Gln}_{CUG}$[M] and tRNA$^{Tyr}_{GUA}$ were expressed individually (along with the EV) in wt and *rps25*$^{\Delta 2-13}$ mutant cells and the SC-RT efficiency on UAG-BSC4 was measured and evaluated as described in Fig. 1b,c; each bar is represented by $n \geq 11$ values. **d**, Model depicting the proposed molecular mechanism of efficient SC-RT. The additional contacts that the rti-tRNAs specifically make with the NTDs of Rps25/eS25 and Rps30/eS30 (marked by yellow asterisks) through their AS increase their odds of being selected during termination to promote efficient SC-RT. Created with BioRender.com.

deletion of the C-terminal pentadecapeptide fragment of Rps15/uS19 does not affect binding of aa-tRNA at the A-site[53]. Furthermore, interactions of the Rps15/uS19 C-terminal tail with the mRNA or the AS of the A-site tRNA are not observed in the eEF1A-bound decoding state[52]. Therefore, it seems plausible that Rps15/uS19 establishes contact with the AS of the A-site tRNA after eEF1A dissociation and kinetic proofreading of the decoded tRNA, which contributes to efficient accommodation of the A-site tRNA, thereby maintaining the optimal rate of elongation. However, this contact may not be of any dramatic importance in the case of near-cognate tRNAs, as these tRNAs would require energetic support mainly during the initial codon sampling phase, which still occurs in the presence of eEF1A.

The N-terminal extension of the Rps25/eS25 was originally thought to be positioned between the P and E sites[54,55]. However, available structures (PDB 7RR5) suggest that it could stretch as far as to the decoding center of the A-site, where it may interact with the first through third base pair of the tRNA AS. So far, the nonessential Rps25/eS25 has been implicated primarily in the translation of a specific population of mRNAs by specialized ribosomes and in the cap-independent translation initiation by internal ribosome entry sites and ribosome shunting[56,57]. However, our data with $tRNA^{Tyr}_{GUA}$ suggest an additional role for this protein in the control of SC-RT and, highly likely, in the aa-tRNA selection process during elongation (Fig. 7d).

Given that nonsense mutations account for approximately 11% of inherited genetic disorders in humans[58], prioritizing SC-RT for nonsense mutation correction represents an attractive approach for treating these disorders that could substantially alleviate human disease[59]. The application of specialized rti-tRNAs engineered to become highly potent for SC-RT, thus, offers a tempting treatment prospect.

Online content

Any methods, additional references, Nature Portfolio reporting summaries, source data, extended data, supplementary information, acknowledgements, peer review information; details of author contributions and competing interests; and statements of data and code availability are available at https://doi.org/10.1038/s41594-024-01450-z.

References

1. Hellen, C. U. T. Translation termination and ribosome recycling in eukaryotes. *Cold Spring Harb. Perspect. Biol.* **10**, a032656 (2018).
2. Floquet, C., Hatin, I., Rousset, J. P. & Bidou, L. Statistical analysis of readthrough levels for nonsense mutations in mammalian cells reveals a major determinant of response to gentamicin. *PLoS Genet.* **8**, e1002608 (2012).
3. Mancera-Martinez, E., Brito Querido, J., Valasek, L. S., Simonetti, A. & Hashem, Y.ABCE1: a special factor that orchestrates translation at the crossroad between recycling and initiation. *RNA Biol.* **14**, 1279–1285 (2017).
4. Heuer, A. et al. Structure of the 40S–ABCE1 post-splitting complex in ribosome recycling and translation initiation. *Nat. Struct. Mol. Biol.* **24**, 453–460 (2017).
5. Becker, T. et al. Structural basis of highly conserved ribosome recycling in eukaryotes and archaea. *Nature* **482**, 501–506 (2012).
6. Palma, M. & Lejeune, F. Deciphering the molecular mechanism of stop codon readthrough. *Biol. Rev. Camb. Philos. Soc.* **96**, 310–329 (2021).
7. Schueren, F. & Thoms, S. Functional translational readthrough: a systems biology perspective. *PLoS Genet.* **12**, e1006196 (2016).
8. Bonetti, B., Fu, L., Moon, J. & Bedwell, D. M. The efficiency of translation termination is determined by a synergistic interplay between upstream and downstream sequences in *Saccharomyces cerevisiae*. *J. Mol. Biol.* **251**, 334–345 (1995).
9. Namy, O., Hatin, I. & Rousset, J. P. Impact of the six nucleotides downstream of the stop codon on translation termination. *EMBO Rep.* **2**, 787–793 (2001).
10. Harrell, L., Melcher, U. & Atkins, J. F. Predominance of six different hexanucleotide recoding signals 3′ of read-through stop codons. *Nucleic Acids Res.* **30**, 2011–2017 (2002).
11. Beznosková, P., Gunišová, S. & Valášek, L. S. Rules of UGA-N decoding by near-cognate tRNAs and analysis of readthrough on short uORFs in yeast. *RNA* **22**, 456–466 (2016).
12. Firth, A. E., Wills, N. M., Gesteland, R. F. & Atkins, J. F. Stimulation of stop codon readthrough: frequent presence of an extended 3′ RNA structural element. *Nucleic Acids Res.* **39**, 6679–6691 (2011).
13. Karijolich, J. & Yu, Y. T. Converting nonsense codons into sense codons by targeted pseudouridylation. *Nature* **474**, 395–398 (2011).
14. Blanchet, S. et al. Deciphering the reading of the genetic code by near-cognate tRNA. *Proc. Natl Acad. Sci. USA* **115**, 3018–3023 (2018).
15. Amrani, N. et al. A faux 3′-UTR promotes aberrant termination and triggers nonsense-mediated mRNA decay. *Nature* **432**, 112–118 (2004).
16. Beznosková, P. et al. Translation initiation factors eIF3 and HCR1 control translation termination and stop codon read-through in yeast cells. *PLoS Genet.* **9**, e1003962 (2013).
17. Beznosková, P., Wagner, S., Jansen, M. E., von der Haar, T. & Valášek, L. S. Translation initiation factor eIF3 promotes programmed stop codon readthrough. *Nucleic Acids Res.* **43**, 5099–5111 (2015).
18. Roy, B., Leszyk, J. D., Mangus, D. A. & Jacobson, A. Nonsense suppression by near-cognate tRNAs employs alternative base pairing at codon positions 1 and 3. *Proc. Natl Acad. Sci. USA* **112**, 3038–3043 (2015).
19. Beznosková, P., Pavlíková, Z., Zeman, J., Echeverria Aitken, C. & Valášek, L. S. Yeast applied readthrough inducing system (YARIS): an invivo assay for the comprehensive study of translational readthrough. *Nucleic Acids Res.* **47**, 6339–6350 (2019).
20. Beznosková, P., Bidou, L., Namy, O. & Valášek, L. S. Increased expression of tryptophan and tyrosine tRNAs elevates stop codon readthrough of reporter systems in human cell lines. *Nucleic Acids Res.* **49**, 5202–5215 (2021).
21. Blanchet, S., Cornu, D., Argentini, M. & Namy, O. New insights into the incorporation of natural suppressor tRNAs at stop codons in *Saccharomyces cerevisiae*. *Nucleic Acids Res.* **42**, 10061–10072 (2014).
22. Ogle, J. M. et al. Recognition of cognate transfer RNA by the 30S ribosomal subunit. *Science* **292**, 897–902 (2001).
23. Ogle, J. M., Murphy, F. V., Tarry, M. J. & Ramakrishnan, V. Selection of tRNA by the ribosome requires a transition from an open to a closed form. *Cell* **111**, 721–732 (2002).
24. Shao, S. et al. Decoding mammalian ribosome–mRNA states by translational GTPase complexes. *Cell* **167**, 1229–1240 (2016).
25. Loveland, A. B., Demo, G., Grigorieff, N. & Korostelev, A. A. Ensemble cryo-EM elucidates the mechanism of translation fidelity. *Nature* **546**, 113–117 (2017).
26. Demeshkina, N., Jenner, L., Westhof, E., Yusupov, M. & Yusupova, G. A new understanding of the decoding principle on the ribosome. *Nature* **484**, 256–259 (2012).
27. Richter, J. D. & Coller, J. Pausing on polyribosomes: make way for elongation in translational control. *Cell* **163**, 292–300 (2015).
28. Stadler, M. & Fire, A. Wobble base-pairing slows in vivo translation elongation in metazoans. *RNA* **17**, 2063–2073 (2011).
29. Budkevich, T. et al. Structure and dynamics of the mammalian ribosomal pretranslocation complex. *Mol. Cell* **44**, 214–224 (2011).
30. Zeng, F. et al. Conserved heterodimeric GTPase Rbg1/Tma46 promotes efficient translation in eukaryotic cells. *Cell Rep.* **37**, 109877 (2021).
31. Bowen, A. M. et al. Ribosomal protein uS19 mutants reveal its role in coordinating ribosome structure and function. *Translation (Austin)* **3**, e1117703 (2015).

32. Kachale, A. et al. Short tRNA anticodon stem and mutant eRF1 allow stop codon reassignment. *Nature* **613**, 751–758 (2023).
33. Pan, T. Modifications and functional genomics of human transfer RNA. *Cell Res.* **28**, 395–404 (2018).
34. Johansson, M.J.O. & Byström, A.S. Transfer RNA modifications and modifying enzymes in *Saccharomyces cerevisiae*. In *Fine-Tuning of RNA Functions by Modification and Editing* (ed. Grosjean, H.) (Springer, 2005).
35. Dabrowski, M., Bukowy-Bieryllo, Z. & Zietkiewicz, E. Translational readthrough potential of natural termination codons in eucaryotes—the impact of RNA sequence. *RNA Biol.* **12**, 950–958 (2015).
36. Nedialkova, D. D. & Leidel, S. A. Optimization of codon translation rates via tRNA modifications maintains proteome integrity. *Cell* **161**, 1606–1618 (2015).
37. Pineyro, D., Torres, A.G. & de Pouplana, L.R. Biogenesis and evolution of functional tRNAs. In *Fungal RNA Biology* (eds Sesma, A. & von der Haar, T.) (Springer, 2014).
38. Lozupone, C. A., Knight, R. D. & Landweber, L. F. The molecular basis of nuclear genetic code change in ciliates. *Curr. Biol.* **11**, 65–74 (2001).
39. Valasek, L. S. et al. Embraced by eIF3: structural and functional insights into the roles of eIF3 across the translation cycle. *Nucleic Acids Res.* **45**, 10948–10968 (2017).
40. Valášek, L., Trachsel, H., Hašek, J. & Ruis, H. Rpg1, the *Saccharomyces cerevisiae* homologue of the largest subunit of mammlian translation initiation factor 3, is required for translational activity. *J. Biol. Chem.* **273**, 21253–21260 (1998).
41. Akhmaloka, Susilowati, Subandi, P. E. & Madayanti, F. Mutation at tyrosine in AMLRY (GILRY like) motif of yeast eRF1 on nonsense codons suppression and binding affinity to eRF3. *Int J. Biol. Sci.* **4**, 87–95 (2008).
42. Panek, T. et al. Nuclear genetic codes with a different meaning of the UAG and the UAA codon. *BMC Biol.* **15**, 8 (2017).
43. Valášek, L. S., Kučerová, M., Zeman, J. & Beznosková, P. Cysteine tRNA acts as a stop codon readthrough-inducing tRNA in the human HEK293T cell line. *RNA* **29**, 1379–1387 (2023).
44. Schultz, D. W. & Yarus, M. tRNA structure and ribosomal function. I. tRNA nucleotide 27–43 mutations enhance first position wobble. *J. Mol. Biol.* **235**, 1381–1394 (1994).
45. Uhlenbeck, O. C. & Schrader, J. M. Evolutionary tuning impacts the design of bacterial tRNAs for the incorporation of unnatural amino acids by ribosomes. *Curr. Opin. Chem. Biol.* **46**, 138–145 (2018).
46. Geslain, R. & Pan, T. Functional analysis of human tRNA isodecoders. *J. Mol. Biol.* **396**, 821–831 (2010).
47. Holm, M. et al. mRNA decoding in human is kinetically and structurally distinct from bacteria. *Nature* **617**, 200–207 (2023).
48. Bulygin, K. N., Graifer, D. M., Hountondji, C., Frolova, L. Y. & Karpova, G. G. Exploring contacts of eRF1 with the 3′-terminus of the P site tRNA and mRNA stop signal in the human ribosome at various translation termination steps. *Biochim. Biophys. Acta* **1860**, 782–793 (2017).
49. Brown, A., Shao, S., Murray, J., Hegde, R. S. & Ramakrishnan, V. Structural basis for stop codon recognition in eukaryotes. *Nature* **524**, 493–496 (2015).
50. Matheisl, S., Berninghausen, O., Becker, T. & Beckmann, R. Structure of a human translation termination complex. *Nucleic Acids Res.* **43**, 8615–8626 (2015).
51. des Georges, A. et al. Structure of the mammalian ribosomal pre-termination complex associated with eRF1·eRF3·GDPNP. *Nucleic Acids Res.* **42**, 3409–3418 (2014).
52. Bhaskar, V. et al. Dynamics of uS19 C-terminal tail during the translation elongation cycle in human ribosomes. *Cell Rep.* **31**, 107473 (2020).
53. Bulygin, K., Malygin, A., Gopanenko, A., Graifer, D. & Karpova, G. The functional role of the C-terminal tail of the human ribosomal protein uS19. *Biochim. Biophys. Acta* **1863**, 194490 (2020).
54. Ben-Shem, A. et al. The structure of the eukaryotic ribosome at 3.0 Å resolution. *Science* **334**, 1524–1529 (2011).
55. Rabl, J., Leibundgut, M., Ataide, S. F., Haag, A. & Ban, N. Crystal structure of the eukaryotic 40S ribosomal subunit in complex with initiation factor 1. *Science* **331**, 730–736 (2011).
56. Hertz, M. I., Landry, D. M., Willis, A. E., Luo, G. & Thompson, S. R. Ribosomal protein S25 dependency reveals a common mechanism for diverse internal ribosome entry sites and ribosome shunting. *Mol. Cell. Biol.* **33**, 1016–1026 (2013).
57. Genuth, N. R. & Barna, M. Heterogeneity and specialized functions of translation machinery: from genes to organisms. *Nat. Rev. Genet.* **19**, 431–452 (2018).
58. Mort, M., Ivanov, D., Cooper, D. N. & Chuzhanova, N. A. A meta-analysis of nonsense mutations causing human genetic disease. *Hum. Mutat.* **29**, 1037–1047 (2008).
59. Valášek, L. S., Lukeš, J. & Paris, Z. Stops making sense—for the people? *Clin. Transl. Med* **13**, e1270 (2023).
60. Chan, P. P. & Lowe, T. M. GtRNAdb 2.0: an expanded database of transfer RNA genes identified in complete and draft genomes. *Nucleic Acids Res.* **44**, D184–D189 (2016).

Methods

S. cerevisiae and *T. brucei* strains and plasmids

The lists and descriptions of all strains, plasmids, primers and GeneArt Strings DNA Fragments (Invitrogen) used throughout this study can be found in Supplementary Tables 1–6.

SC-RT assays

The majority of SC-RT assays in this study were performed using a standard bicistronic reporter construct bearing a *Renilla* luciferase gene followed by an in-frame firefly luciferase gene, originally developed in a previous study[61]. The two genes are separated by either a tetranucleotide termination signal (UGA-C) or, for control purposes, the CAA sense codon, followed by cytosine. In indicated cases, the termination signal and/or the following nucleotide context was modified. Note that mRNA levels of the reporters bearing the stop signal between *Renilla* and firefly genes do not differ from the CAA sense control[19]. This system avoids possible artifacts connected to the changes in the efficiency of translation initiation associated with the nonsense-mediated decay pathway[62], because both *Renilla* and firefly enzymes initiate translation from the same AUG codon. All experiments and data analyses were carried out according to the microtiter plate-based dual-luciferase assay (Promega). Readthrough measurements were conducted from at least three biological replicates ($n \geq 3$) and each experiment was repeated 2–5 times (no technical replicates were carried out). The readthrough values (shown as individual dots) are represented by bars illustrating the mean value ± s.d. Statistical significance was determined using the nonparametric Mann–Whitney test in R statistical software (version 4.3.0; www.r-project.org). The readthrough and statistical calculations with raw data of firefly and *Renilla* measurements are given in the Source Data.

Northern blot analysis

To examine the expression levels of studied tRNAs, total RNA from yeast was isolated by the quick RNA miniprep assay and total RNA from *T. brucei* was isolated as previously described[63]. Briefly, 1 µg (*S. cerevisiae*) or 10 µg (*T. brucei*) was separated on a denaturing 8 M urea 8% polyacrylamide gel and electroblotted to zeta-probe membranes. The membrane was then crosslinked under ultraviolet (UV) light for 1 min followed by northern hybridization according to the manufacturer (Bio-Rad) using with ^{32}P-labeled oligonucleotides. Following hybridization, membranes were exposed overnight on a phosphoimager screen. Blots were analyzed using a Typhoon scanner and the ImageQuant TL software (GE Healthcare).

Polysomal gradient analysis

The *S. cerevisiae* strains bearing the wt or mutant Rps30/eS30 were cultured in yeast peptone dextrose (YPD) medium at 30 °C to an optical density at 600 nm of ~0.5. Cycloheximide (50 µg ml^{-1}) was added 5 min before harvesting by centrifugation at 1,455*g* for 5 min at 4 °C. The whole-cell extracts (WCEs) were prepared in the Ga–HEPES buffer composed of 10 mM HEPES (pH 7.5), 62.5 mM KCl and 10 mM $MgCl_2$ supplemented with 50 µg ml^{-1} cycloheximide, 1 mM DTT, 1 mM PMSF and one tablet of cOmplete EDTA-free protease inhibitor cocktail per 25 ml of buffer. Cells were broken using glass beads (~1/2 volume) with a bead beater homogenizer. After centrifugation at 15,871*g* for 5 min at 4 °C, the supernatant was transferred into a precooled 1.5-ml tube and cleared by centrifugation at 21,130*g* at 4 °C for 10 min.

For polysome profile analysis, 15 A_{260} units of WCEs were separated by high velocity sedimentation on a 5–45% sucrose gradient in Ga–HEPES buffer by centrifugation at 39,000*g* at 4 °C for 2.5 h in an SW41Ti rotor (Beckman Coulter). The resulting gradients were scanned at A_{254} using a Teledyne ISCO UA-6 UV–visible light gradient detector.

For the 60S:40S ratio analysis, 15 A_{260} units of WCEs with the addition of 50 mM EDTA were separated and analyzed as described above in Ga–HEPES buffer without $MgCl_2$ to visualize free 40S and 60S ribosomal subunits.

Bioinformatics

The genomes and protein-coding sequences were collected from the National Center for Biotechnology Information and are listed in Supplementary Table 7a. The tRNAs^{Gln} were predicted by ARAGORN (version 1.2.38)[64] and tRNAscan-SE (version 2.0.5)[65]. Identical sequences of one organism were deduplicated using an in-house python script (https://github.com/kikinocka/ngs/blob/master/py_scripts/deduplicate_sequence_seqs.py). This means that there were still some identical sequences in the dataset but originating from different assemblies. Sequences from ciliates with canonical genetic code (alignment file 1) and those with reassigned TAR codons (alignment file 2) were aligned separately using MAFFT G-INS-i (version 7.458)[66]. Sequences with a longer variable loop were manually refined using secondary structures obtained from ARAGORN and/or tRNAscan-SE. The base pair corresponding to the 28:42 base pair was extracted from the alignments (Supplementary Table 7b) using an in-house python script (https://github.com/kikinocka/ngs/blob/master/py_scripts/nt_pair_aln.py). Codon usage of each protein-coding sequence was determined using an in-house python script (https://github.com/kikinocka/ngs/blob/master/py_scripts/codon_usage.py). The total sum of each glutamine codon was extracted for each organism as observed numbers; the expected numbers were calculated as (CAA + CAG + TAA + TAG)/4 and a chi-square test was conducted (Supplementary Table 7c)[67].

Statistics and reproducibility

Each bar is represented by readthrough values (that is, individual biological replicates shown as dots) and illustrates the mean value ± s.d. Statistical significance was determined using the nonparametric Mann–Whitney test (****$P < 0.0001$, ***$P < 0.001$, **$P < 0.01$ and *$P < 0.05$). Data for the firefly and *Renilla* measurements, additional measurements and statistical calculations are provided in the Source Data.

Reporting summary

Further information on research design is available in the Nature Portfolio Reporting Summary linked to this article.

Data availability

All data generated during this study are included in this published article and the Supplementary Information. Published datasets included in the study were obtained from the PDB under accession numbers 5LZS and 7RR5. Source data are provided with this paper.

References

61. Grentzmann, G., Ingram, J. A., Kelly, P. J., Gesteland, R. F. & Atkins, J. F. A dual-luciferase reporter system for studying recoding signals. *RNA* **4**, 479–486 (1998).
62. Muhlrad, D. & Parker, R. Recognition of yeast mRNAs as 'nonsense containing' leads to both inhibition of mRNA translation and mRNA degradation: implications for the control of mRNA decapping. *Mol. Biol. Cell* **10**, 3971–3978 (1999).
63. Chomczynski, P. & Sacchi, N. The single-step method of RNA isolation by acid guanidinium thiocyanate–phenol–chloroform extraction: twenty-something years on. *Nat. Protoc.* **1**, 581–585 (2006).
64. Laslett, D. & Canback, B. ARAGORN, a program to detect tRNA genes and tmRNA genes in nucleotide sequences. *Nucleic Acids Res.* **32**, 11–16 (2004).
65. Chan, P. P., Lin, B. Y., Mak, A. J. & Lowe, T. M. tRNAscan-SE 2.0: improved detection and functional classification of transfer RNA genes. *Nucleic Acids Res.* **49**, 9077–9096 (2021).
66. Katoh, K. & Standley, D. M. MAFFT multiple sequence alignment software version 7: improvements in performance and usability. *Mol. Biol. Evol.* **30**, 772–780 (2013).
67. Slabodnick, M. M. et al. The macronuclear genome of stentor coeruleus reveals tiny introns in a giant cell. *Curr. Biol.* **27**, 569–575 (2017).

Acknowledgements
We are grateful to Š. Coufal (Institute of Microbiology CAS, Prague) for his help with statistical analysis, to I. Malcová (Institute of Microbiology CAS, Prague) and J. D. Dinman (University of Maryland) for providing various plasmids and to S. Leidel (University of Bern) for providing yeast strains individually deleted for genes required for the U_{34} modification. We are also thankful to two of three main reviewers and the arbitrating referee with expertise in biostatistics for their constructive comments and continuous and very encouraging support throughout an entire review process. This work was supported by the Czech Science Foundation grants 20-00579S (to L.S.V.) and 20-11585S (to Zd.Pa.), Lead Agency grant 23-08669L (to L.S.V. and Zd.Pa.), Praemium Academiae grant provided by the Czech Academy of Sciences (to L.S.V.) and the Charles University Grant Agency project GA UK 1192819 (to Zu.Pa.). Computational resources were provided by e-INFRA CZ project 90140, supported by the Ministry of Education, Youth and Sports of the Czech Republic.

Author contributions
Zu.Pa., P.B. and L.S.V. conceptualized and designed the project. Zu.Pa., P.M., K.P., A.R., K.Z., I.M.D., A.K. and Zd.Pa. carried out all experiments and performed the data analysis. Zu.Pa., P.M., Zd.Pa., P.B. and L.S.V. interpreted the results. L.S.V. wrote the paper with input from Zu.Pa., P.M., K.Z., T.B., J.L., Zd.Pa. and P.B.

Competing interests
The authors declare no competing interests.

Additional information
Extended data is available for this paper at https://doi.org/10.1038/s41594-024-01450-z.

Supplementary information The online version contains supplementary material available at https://doi.org/10.1038/s41594-024-01450-z.

Correspondence and requests for materials should be addressed to Leoš Shivaya Valášek.

Peer review information *Nature Structural & Molecular Biology* thanks the anonymous reviewers for their contribution to the peer review of this work. Peer reviewer reports are available. Primary Handling Editor: Sara Osman and Dimitris Typas, in collaboration with the *Nature Structural & Molecular Biology* team.

https://doi.org/10.1038/s41594-024-01450-z

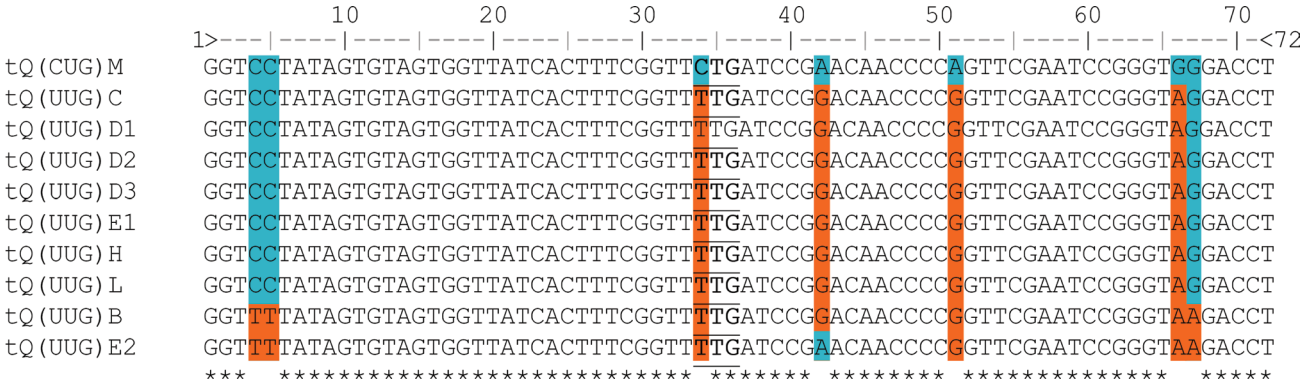

Extended Data Fig. 1 | Multiple sequence alignment of *S. cerevisiae* tRNA^{Gln} iso-acceptors retrieved from the GtRNAdb. Variable positions among iso-acceptors are highlighted by colors; same residues with tRNA$^{Gln}_{CUG}$[M] in blue, differing residues in orange.

https://doi.org/10.1038/s41594-024-01450-z

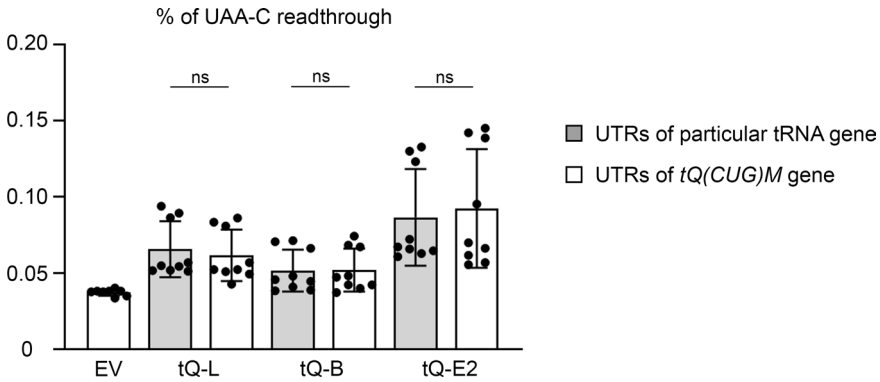

Extended Data Fig. 2 | UTRs of tRNA^{Gln} iso-acceptors do not influence SC-RT efficiency. The wt tRNA$^{Gln}_{UUG}$ iso-decoders flanked by either the genuine or "tRNA$^{Gln}_{CUG}$[M]" UTRs were expressed individually (along with EV) in wt yeast cells and the efficiency of SC-RT on UAA-C was measured and evaluated as described in Fig. 1b – c; each bar is represented n ≥ 8 values; that is individual biological replicates shown as dots.

https://doi.org/10.1038/s41594-024-01450-z

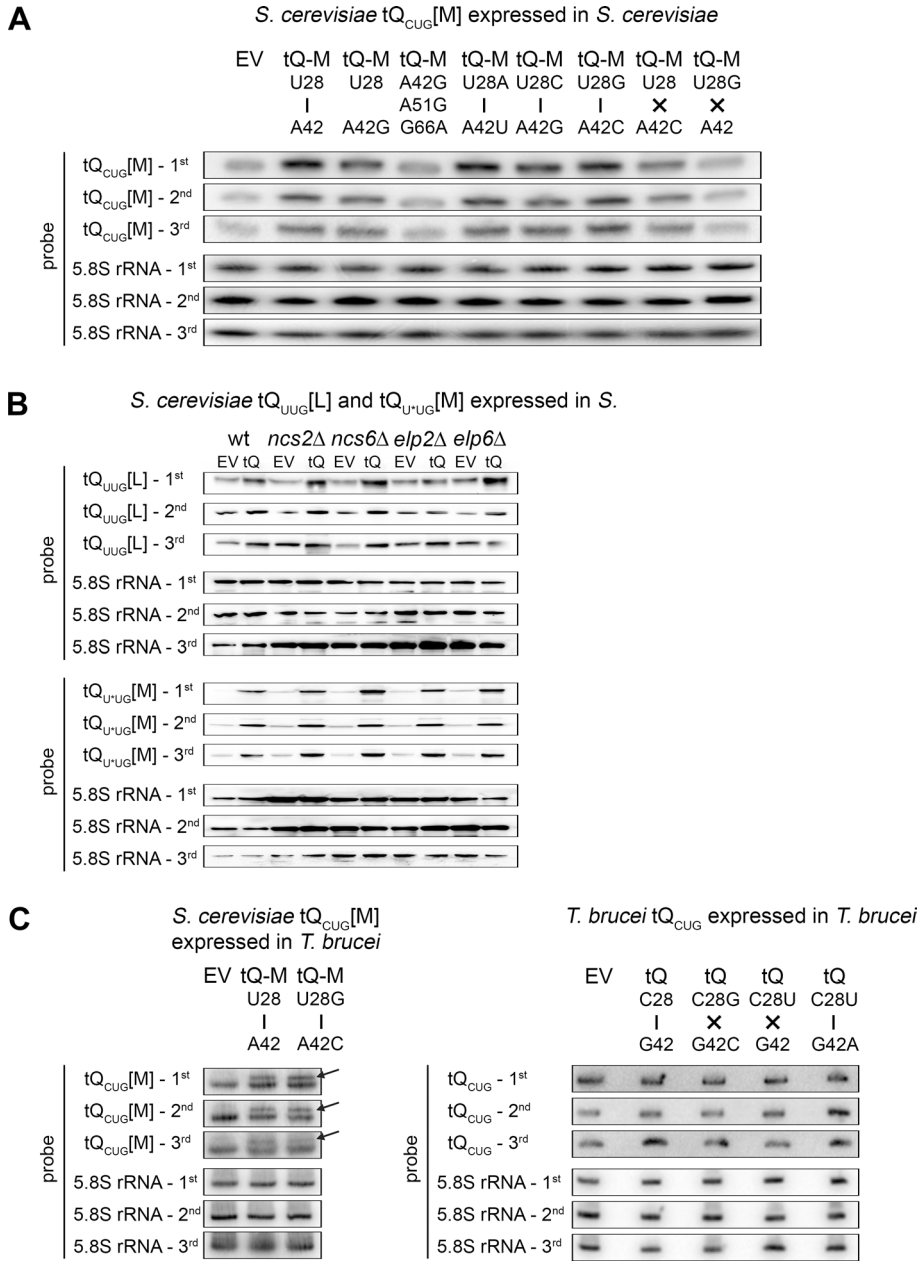

Extended Data Fig. 3 | Expression levels of tRNA^{Gln} variants in *S. cerevisiae* and *T. brucei*. (**A**) Expression of the *S. cerevisiae* tRNA$^{Gln}_{CUG}$ [M] variants in *S. cerevisiae*. Total RNA was isolated from the wt *S. cerevisiae* strain PBH156 expressing plasmid-borne high copy wt or indicated mutant variants of tRNA$^{Gln}_{CUG}$ (tQ-M; indicated at the top of each panel). Five micrograms of total RNA was resolved on the urea gel, transferred onto a nylon membrane and hybridized with a specific [γ^{32}P]ATP labeled probe against tRNA$^{Gln}_{CUG}$ [M]. The 5.8S rRNA was used as a loading control. Three biological replicates are shown; for quantifications, see Source Data Extended Data Fig. 3. For gel source data, see Supplementary Information. (**B**) Expression of the *S. cerevisiae* tRNA$^{Gln}_{UUG}$[L] and tRNA$^{Gln}_{U*UG}$[M] variants in *S. cerevisiae*. Total RNA was isolated from the indicated wt and mutant *S. cerevisiae* strains expressing either empty vector or tRNA$^{Gln}_{UUG}$[L] (upper 6 panels) or tRNA$^{Gln}_{U*UG}$[M] (lower 6 panels). One microgram of total RNA was resolved on the urea gel, transferred onto a nylon membrane and hybridized with a specific DIG-labeled probe against tRNA$^{Gln}_{CUG}$ [M]. The 5.8S rRNA was used as a loading control. For details see the main text and Fig. 1E and F. Three biological replicates are shown; for quantifications, see Source Data Extended Data Fig. 3. For gel source data, see Supplementary Information. (**C**) Expression of the *S. cerevisiae* tRNA$^{Gln}_{CUG}$[M] and *T. brucei* tRNA$^{Gln}_{CUG}$ variants in *T. brucei*. (left) Total RNA was extracted from *T. brucei* strain 29-13 expressing the genome integrated plasmid pLEW100 bearing (tQ) variants from *S. cerevisiae* (indicated at the top of each panel). Ten µg of RNA was resolved by urea-PAGE, followed by the northern blot analysis using [γ^{32}P]ATP labeled oligonucleotide specific for both tQ variants; Empty vector (EV) served as a negative control. 5.8S rRNA was used as a loading control. Three biological replicates are shown. (right) Total RNA was extracted from *T. brucei* strain 29-13 expressing the genome integrated plasmid pLEW100 bearing (tQ) variants from *T. brucei* (indicated at the top of each panel). Ten µg of RNA was resolved by urea-PAGE, followed by the northern blot analysis using [γ^{32}P]ATP labeled oligonucleotide specific for tQ variants; Empty vector (EV) served as a negative control. 5.8S rRNA was used as a loading control. Three biological replicates are shown. For gel source data, see Supplementary Information.

https://doi.org/10.1038/s41594-024-01450-z

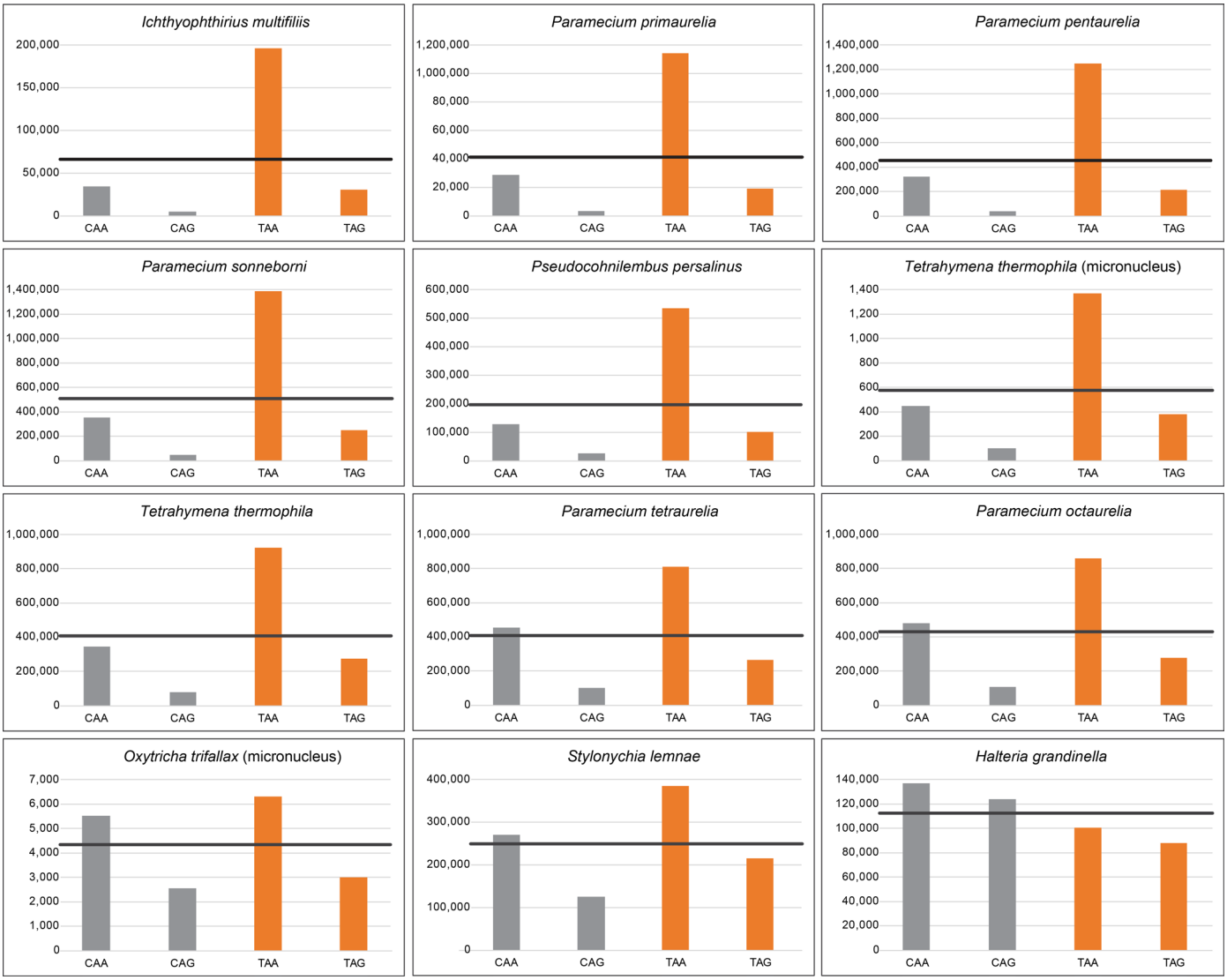

Extended Data Fig. 4 | Codon usage of Gln codons in ciliates with reassigned genetic code. Protein-coding sequences originating from macronucleus (unless stated otherwise) were obtained from NCBI (Extended Data Supplementary Excel file 1A). Codon usage of all Gln codons (CAA, CAG, TAA, and TAG) was determined (Extended Data Supplementary Excel file 1 C), and the observed numbers were visualized as bar plots. Expected numbers ([CAA + CAG + TAA + TAG]/4) are represented by horizontal black lines. Canonical and reassigned Gln codons are in grey and orange, respectively.

https://doi.org/10.1038/s41594-024-01450-z

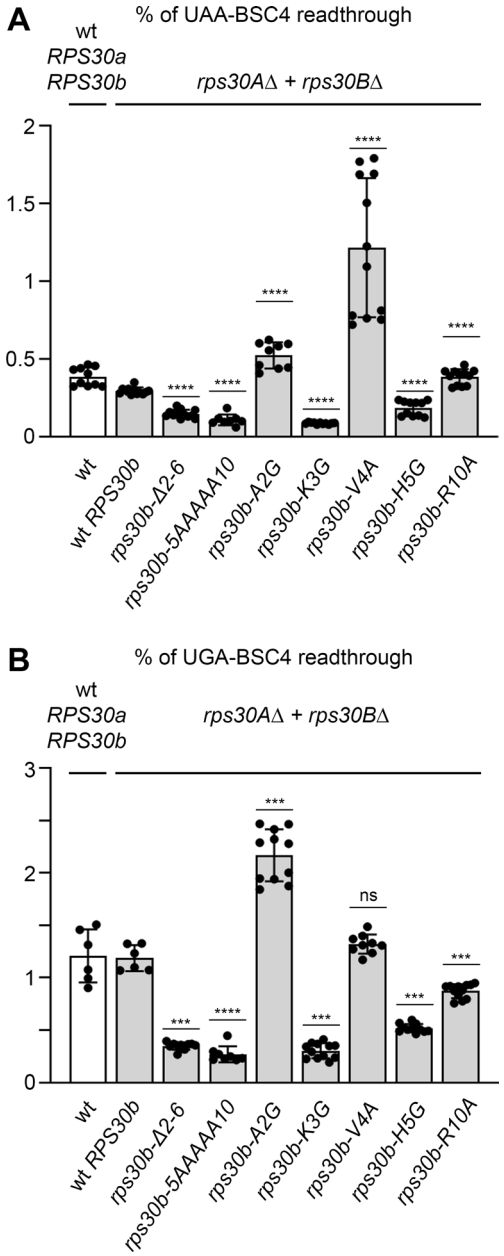

Extended Data Fig. 5 | Rps30/eS30 mutants differentially modulate the SC-RT efficiency at the UAA and UGA stop codon. (**A** – **B**). The wt and indicated Rps30/eS30 mutant yeast cells were examined for efficiency of SC-RT on (**A**) UAA-BSC4 or (**B**) UGA-BSC4 as described in Fig. 1b – c; each bar is represented by (**A**) n ≥ 9 or (**B**) n ≥ 6 readthrough values; that is individual biological replicates shown as dots.

https://doi.org/10.1038/s41594-024-01450-z

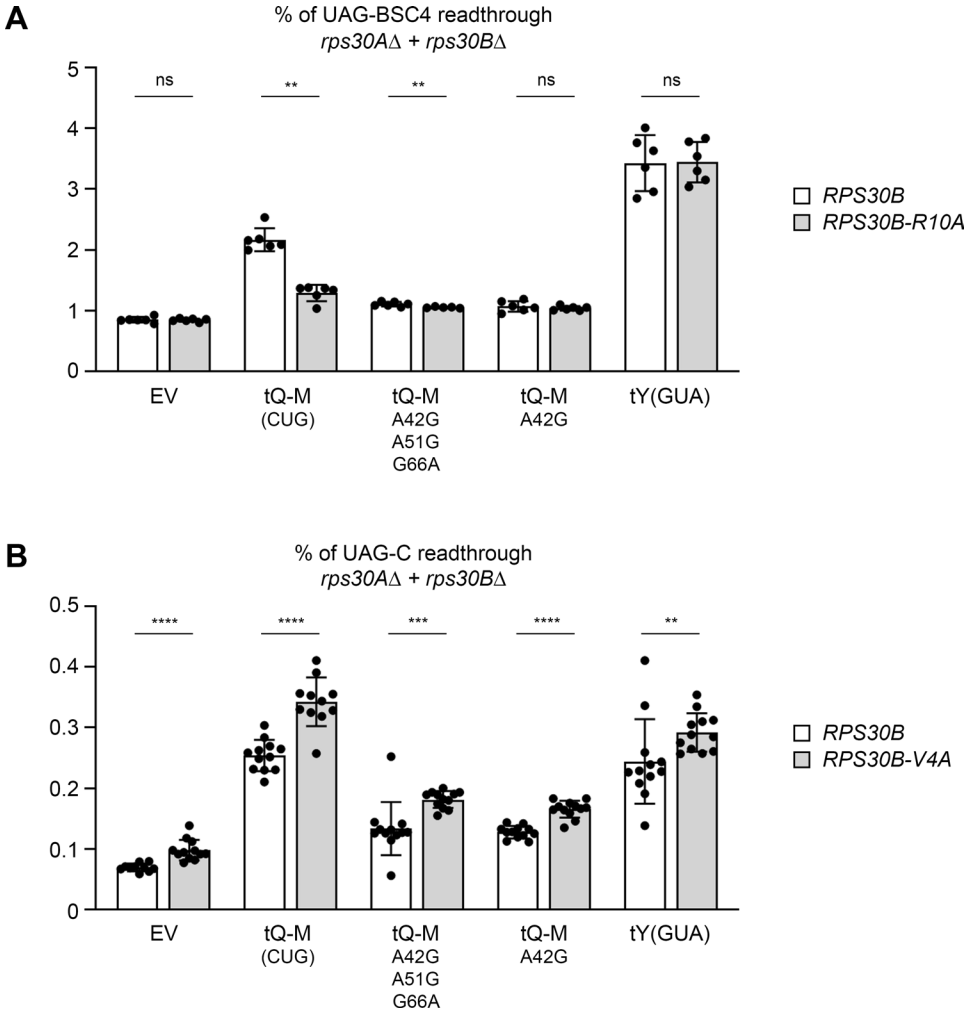

Extended Data Fig. 6 | Impact of the Rps30/eS30 mutants on incorporation of the tRNA$^{Gln}_{CUG}$[M] iso-acceptor into the A site. (**A**) R10 of Rps30/eS30 may potentiate the SC-RT-promoting ability of tRNA$^{Gln}_{CUG}$[M] by directly contacting the 28:42 base pair of its AS. The wt and indicated mutant variants of the tRNA$^{Gln}_{CUG}$[M] iso-acceptor, as well as control tRNA$^{Tyr}_{GUA}$ were expressed individually (along with EV) in wt and *rps30B-R10A* mutant yeast cells and the efficiency of SC-RT on UAG-BSC4 was measured and evaluated as described in Fig. 1b - c; each bar is represented by n ≥ 5 values; that is individual biological replicates shown as dots. (**B**) V4 of Rps30/eS30 has no effect on the SC-RT-promoting ability of tRNA$^{Gln}_{CUG}$[M]. The same as in panel A only the *V4A* instead of *R10A* mutation of Rps30/eS30 was examined on UAG-C; each bar is represented n ≥ 10 values; that is individual biological replicates shown as dots.

https://doi.org/10.1038/s41594-024-01450-z

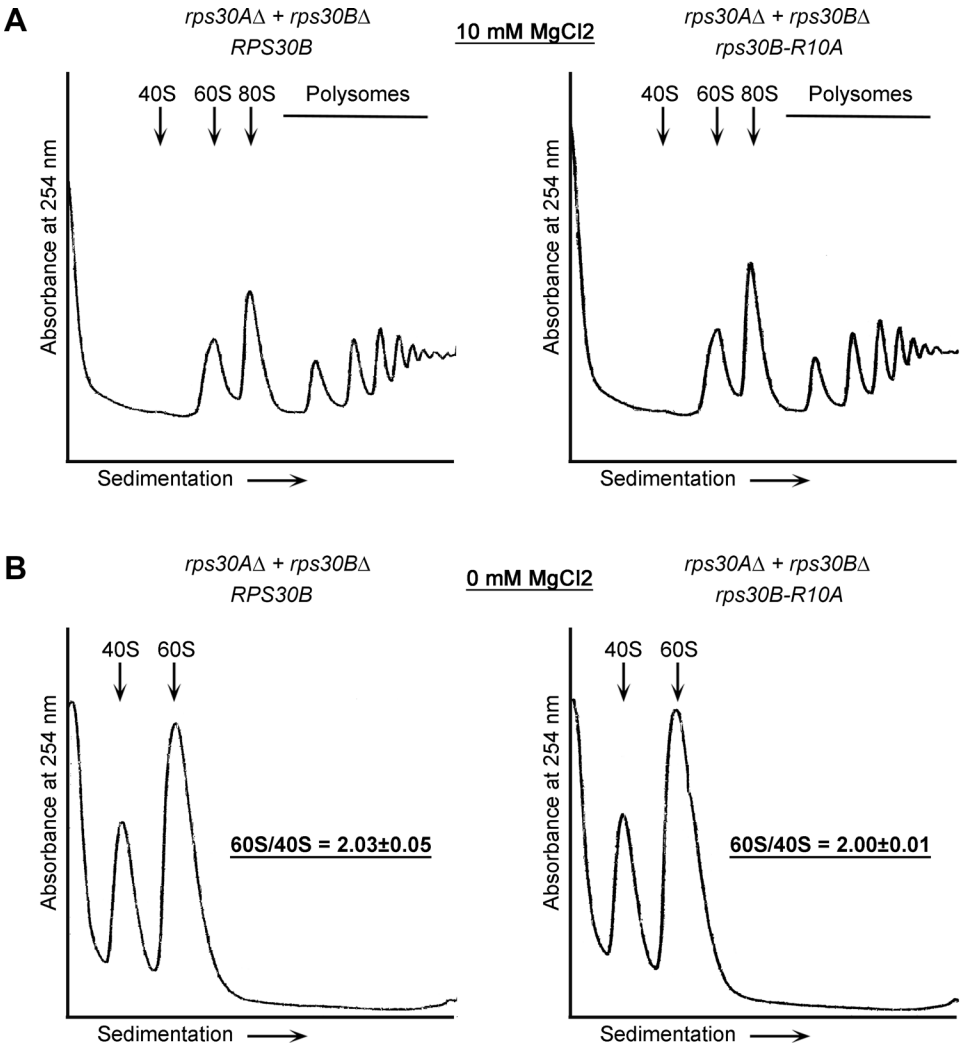

Extended Data Fig. 7 | The Rps30/eS30 mutation *R10A* has no detectable impact either on the polysome content or on the 60S/40S ratio. (**A** – **B**) Polysomal profiles of wt vs. *rps30B-R10A* mutant yeast cells (**A**) in the presence of 10 mM $MgCl_2$ or (**B**) in the absence of $MgCl_2$. Yeast cells bearing the indicated wt or mutant Rps30/eS30 were grown in the YPD medium at 30 °C to an OD_{600} ~ 0.5 and processed for polysomal gradient analysis as described in Methods. Positions of 40S, 60S and 80S species are indicated by arrows; polysomes by a horizontal line. (**B**) The 60S/40S ratio represents the result from three independent experiments ± SD.

https://doi.org/10.1038/s41594-024-01450-z

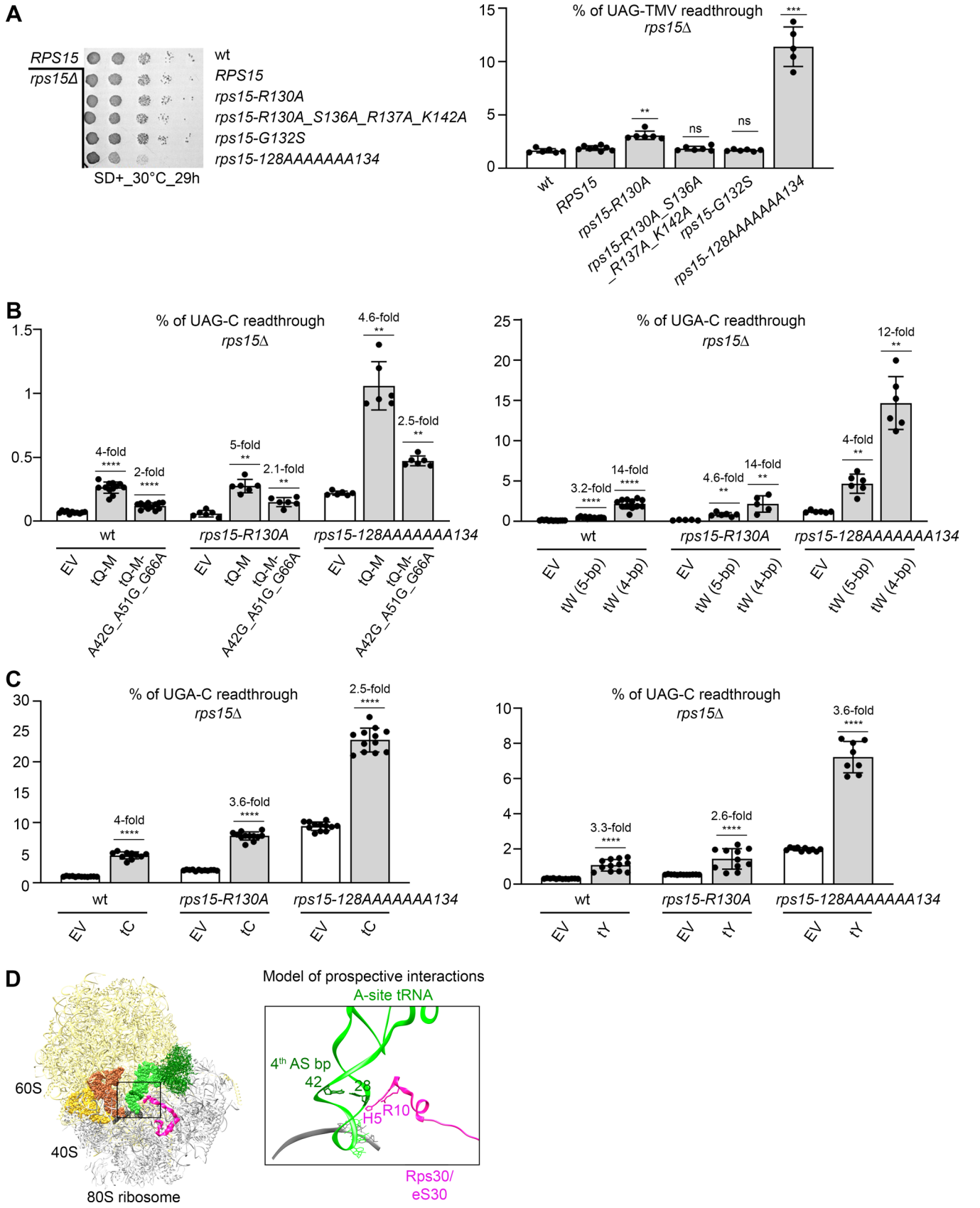

Extended Data Fig. 8 | See next page for caption.

https://doi.org/10.1038/s41594-024-01450-z

Extended Data Fig. 8 | The extreme C-terminal residues of Rps19/uS19 do not influence the SC-RT efficiency of any rti-tRNAs or their mutant variants. (**A**, left) Growth rate and stop codon readthrough analysis of the C-terminal substitution mutants of Rps15/uS19. The wt and indicated Rps15/uS19 mutant yeast cells were spotted in five serial 10-fold dilutions on minimal media supplemented with required aa and incubated for 29 hours at 30 °C. (**A**, right) The same cells were tested for efficiency of SC-RT in the UAG-TMV stop codon context as described in Fig. 1b - c; each bar is represented by n ≥ 6 values; that is individual biological replicates shown as dots. (**B**) The extreme C-terminal residues of Rps15/uS19 do not influence the SC-RT efficiency of $tRNA^{Gln}_{CUG}$[M] and $tRNA^{Trp}_{CCA}$ or their mutant variants. The wt and indicated mutant variants of $tRNA^{Gln}_{CUG}$[M] (left) and $tRNA^{Trp}_{CAA}$ (right) were expressed individually (along with EV) in wt and indicated *rps15* mutant yeast cells and the efficiency of SC-RT on UAG-C and UGA-C, respectively, was measured and evaluated as described in Fig. 1b – c; each bar is represented by n ≥ 6 values; that is individual biological replicates shown as dots. (**C**) The extreme C-terminal residues of Rps15/uS19 do not influence the SC-RT efficiency of $tRNA^{Tyr}_{GUA}$ and $tRNA^{Cys}_{GCA}$. The wt $tRNA^{Cys}_{GCA}$ (left) and $tRNA^{Tyr}_{GUA}$ (right) were expressed individually (along with EV) in wt and indicated *rps15* mutant yeast cells and the efficiency of SC-RT on UGA-C and UAG-C, respectively, was measured and evaluated as described in Fig. 1b – c; each bar is represented by (left panel) n ≥ 10 or (right panel) n ≥ 8 readthrough values; that is individual biological replicates shown as dots. (**D**) Model of the rabbit 80S ribosome (PDB-ID 5LZS; left) zoomed-in to highlight the A site (right). Shown are the prospective contacts between the 4th base-pair of the tRNA AS and the ribosomal protein Rps30/eS30 in the A site. The A-site tRNA is shown in green (the 4th base-pair of its AS in dark green) and Rps30/eS30 in magenta with His5 and Arg10 highlighted.

https://doi.org/10.1038/s41594-024-01450-z

Extended Data Table 1 | The 28:42 base pair counts in $tRNAs^{Gln}$ of ciliates with canonical genetic code (UAR = stop) and those with reassigned UAR codons (UAR=Q)

	28:42 pair	count	total	ratio
UAR = Q – CTG				
pyrimidine : purine	T:A	4	11	**1**
	C:G	7		
purine : pyrimidine	A:T	28	31	**3**
	G:C	1		
pyrimidine : purine (no pair)	T:G	1		
purine : purine (no pair)	A:A	1		
UAR = stop – CTG				
pyrimidine : purine	T:A	3	11	**1**
	C:G	8		
purine : pyrimidine	A:T	7	10	**1**
	G:C	1		
	G:T	1		
UAR = Q – TTG				
pyrimidine : purine	T:A	32	61	**2**
	C:G	29		
purine : pyrimidine	A:T	11	30	**1**
	G:C	18		
pyrimidine : purine (no pair)	T:G	1		
UAR = stop – TTG				
pyrimidine : purine	T:A	6	12	**1**
	C:G	6		
purine : pyrimidine	A:T	4	21	**2**
	G:C	17		

nature portfolio

Corresponding author(s): Leos Valasek

Last updated by author(s): 2024-6-2

Reporting Summary

Nature Portfolio wishes to improve the reproducibility of the work that we publish. This form provides structure for consistency and transparency in reporting. For further information on Nature Portfolio policies, see our Editorial Policies and the Editorial Policy Checklist.

Statistics

For all statistical analyses, confirm that the following items are present in the figure legend, table legend, main text, or Methods section.

n/a	Confirmed	
☐	☒	The exact sample size (*n*) for each experimental group/condition, given as a discrete number and unit of measurement
☐	☒	A statement on whether measurements were taken from distinct samples or whether the same sample was measured repeatedly
☐	☒	The statistical test(s) used AND whether they are one- or two-sided *Only common tests should be described solely by name; describe more complex techniques in the Methods section.*
☐	☒	A description of all covariates tested
☐	☒	A description of any assumptions or corrections, such as tests of normality and adjustment for multiple comparisons
☐	☒	A full description of the statistical parameters including central tendency (e.g. means) or other basic estimates (e.g. regression coefficient) AND variation (e.g. standard deviation) or associated estimates of uncertainty (e.g. confidence intervals)
☐	☒	For null hypothesis testing, the test statistic (e.g. *F*, *t*, *r*) with confidence intervals, effect sizes, degrees of freedom and *P* value noted *Give P values as exact values whenever suitable.*
☒	☐	For Bayesian analysis, information on the choice of priors and Markov chain Monte Carlo settings
☒	☐	For hierarchical and complex designs, identification of the appropriate level for tests and full reporting of outcomes
☒	☐	Estimates of effect sizes (e.g. Cohen's *d*, Pearson's *r*), indicating how they were calculated

Our web collection on statistics for biologists contains articles on many of the points above.

Software and code

Policy information about availability of computer code

Data collection	No software was used for data collection.
Data analysis	ARAGORN v1.2.38 tRNAscan-SE v2.0.5 MAFFT v7.458 R statistical software (version 4.3.0. www.r-project.org) MS Excel Professional Plus 2016 ImageQuant TL software (GE Healthcare) in-house python script (https://github.com/kikinocka/ngs/blob/master/py_scripts/deduplicate_sequence_seqs.py) in-house python script (https://github.com/kikinocka/ngs/blob/master/py_scripts/nt_pair_aln.py) in-house python script (https://github.com/kikinocka/ngs/blob/master/py_scripts/codon_usage.py).

For manuscripts utilizing custom algorithms or software that are central to the research but not yet described in published literature, software must be made available to editors and reviewers. We strongly encourage code deposition in a community repository (e.g. GitHub). See the Nature Portfolio guidelines for submitting code & software for further information.

Data

Policy information about availability of data

All manuscripts must include a data availability statement. This statement should provide the following information, where applicable:

- Accession codes, unique identifiers, or web links for publicly available datasets
- A description of any restrictions on data availability
- For clinical datasets or third party data, please ensure that the statement adheres to our policy

All data generated during this study are included in this published article (and its Supplementary Information files). Published data sets included in the study: PDB-ID 5LZS and PDB-ID 7RR5.

Research involving human participants, their data, or biological material

Policy information about studies with human participants or human data. See also policy information about sex, gender (identity/presentation), and sexual orientation and race, ethnicity and racism.

Reporting on sex and gender	N/A
Reporting on race, ethnicity, or other socially relevant groupings	N/A
Population characteristics	N/A
Recruitment	N/A
Ethics oversight	N/A

Note that full information on the approval of the study protocol must also be provided in the manuscript.

Field-specific reporting

Please select the one below that is the best fit for your research. If you are not sure, read the appropriate sections before making your selection.

☒ Life sciences ☐ Behavioural & social sciences ☐ Ecological, evolutionary & environmental sciences

For a reference copy of the document with all sections, see nature.com/documents/nr-reporting-summary-flat.pdf

Life sciences study design

All studies must disclose on these points even when the disclosure is negative.

Sample size	Readthrough measurements were conducted with at least three biological replicates (n ≥ 3) and each experiment was repeated from 2 to 5 times (no technical replicates were carried out), which is the standard in the field. The number of repeats N is defined in each figure legend. Samples were chosen based on the commonly used standards in the very field; no data were excluded.
Data exclusions	no data was excluded
Replication	all findings are easily reproducible and were conducted with at least three biological replicates (n ≥ 3) and each experiment was repeated from 2 to 5 times (no technical replicates were carried out)
Randomization	this is not relevant because no experimental groups of organisms were generated in our study
Blinding	All the experiments did not involve any blinding measurements, because it is not technically doable/required for these types of analyses.

Reporting for specific materials, systems and methods

We require information from authors about some types of materials, experimental systems and methods used in many studies. Here, indicate whether each material, system or method listed is relevant to your study. If you are not sure if a list item applies to your research, read the appropriate section before selecting a response.

Materials & experimental systems

n/a	Involved in the study
☒	☐ Antibodies
☒	☐ Eukaryotic cell lines
☒	☐ Palaeontology and archaeology
☒	☐ Animals and other organisms
☒	☐ Clinical data
☒	☐ Dual use research of concern
☒	☐ Plants

Methods

n/a	Involved in the study
☒	☐ ChIP-seq
☒	☐ Flow cytometry
☒	☐ MRI-based neuroimaging